Stochastic Analysis of the Electromagnetic Induction Effect on a Neuron's Action Potential Dynamics

Ante Lojic Kapetanovic (alojic00@fesb.hr)
University of Split: Sveuciliste u Splitu https://orcid.org/0000-0001-5507-5788
Anna Susnjara
University of Split: Sveuciliste u Splitu
Dragan Poljak
University of Split: Sveuciliste u Splitu

Research Article

Keywords: conductance-based neuron model, memristor coupling, electromagnetic induction, uncertainty quantification, stochastic sensitivity analysis

Posted Date: March 8th, 2021

DOI: https://doi.org/10.21203/rs.3.rs-280952/v1

Version of Record: A version of this preprint was published at Nonlinear Dynamics on August 7th, 2021.
See the published version at https://doi.org/10.1007/s11071-021-06762-z.

Nonlinear Dynamics manuscript No.
(will be inserted by the editor)

Stochastic analysis of the electromagnetic induction effect on a neuron's action potential dynamics

Ante Lojić Kapetanović · Anna Šušnjara · Dragan Poljak

Received: date / Accepted: date

Abstract This paper examines the effect of electromagnetic induction on the electrophysiology of a single cortex neuron through two different modes associated with the nature of the external neuronal stimulus. By using the recently extended induction-based variant of the well-known and biologically plausible Hodgkin-Huxley neuron model, bifurcation analysis is performed. Electromagnetic induction caused by magnetic flux is captured using a polynomial approximation of a memristor embedded into the neuron model. In order to determine true influence of the variability of ion channels conductivity, the stochastic sensitivity analysis is performed *post hoc*. Additionally, numerical simulations are enriched with uncertainty quantification, observing values of ion channels conductivity as random variables. The aim of the study is to computationally determine the sensitivity of the action potential dynamics with respect to the changes in conductivity of each ion channel so that the future experimental procedures, most often medical treatments, may be adapted to different individuals in various environmental conditions.

A. L. Kapetanović ✉
E-mail: alojic00@fesb.hr
Department of Electronics and Computing
University of Split
Rudera Boskovica 32
21000 Split, Croatia

A. Šušnjara
Department of Electronics and Computing
University of Split
Rudera Boskovica 32
21000 Split, Croatia

D. Poljak
Department of Electronics and Computing
University of Split
Rudera Boskovica 32
21000 Split, Croatia

Keywords conductance-based neuron model · memristor coupling · electromagnetic induction · uncertainty quantification · stochastic sensitivity analysis

1 Introduction

The electromagnetic influence on human tissue and organs is most often observed through two frameworks: low frequency effects on the nervous system (a change in the action potential dynamics of the neuronal membrane) and thus on brain metabolism, and radiofrequency thermal effects. Recently published guidelines for limiting exposure to electromagnetic fields by International Commission on Non-Ionizing Radiation Protection (ICNIRP) [18] state that the only effect at frequencies of 10 MHz or higher is human or organ heating, though some authors claim that even on such high frequencies, given that the incident power density is sufficiently low, it is possible to observe ultrasonic vibrations in the membrane of a neuron as a result of interaction with electromagnetic radiation [44], which is supported experimentally [36]. However, the most of the literature defines clear boundaries between the influence of low-frequency radiation (up to 100 kHz) and radiofrequency radiation (100 kHz to 300 GHz), where for the range from 100 kHz to 10 MHz, the possibility of influence of neuronal stimulation and tissue heating both exists [39]. In summary, as the radiation frequency increases, heating effects predominate and the likelihood of nerve stimulation decreases. A detailed review of neurobehavior during exposure to low-frequency electric and magnetic fields is given in [17]. In this paper, we are concentrated on the effects of time-varying magnetic fields where the main interaction is the Faraday induction of electrical fields and associated currents, the value of which depends on the tissue configuration, orientation and conductivity. The electro-stimulation of a neuron, the electrical polarization

of presynaptic processes leading to a change in post synaptic cell activity, is examined using a computational neuron model extended with an additive variable which is capable of capturing the effect of electromagnetic induction.

Extensive research has been carried out w.r.t. magnetic stimulation of a neuron and neuronal network through clinical studies and computer simulations, respectively [3, 34, 35]. The treatment of the neurodegenerative diseases in the context of electromagnetic induction is also discussed, e.g., for Alzheimer disease [4], and for epilepsy [10]. The effectiveness of electromagnetic stimulation in the treatment of mental illnesses is computationally assessed in [23] through the regulatory abilities of the external electromagnetic stimulation on the pattern dynamics of neuronal networks.

Much effort has been invested in realization of very precise numerical models of a neuron as well, from simple models such as integrate-and-fire [15] and associated extensions [9, 19, 45], over more bio-physically realistic models such as Hodgkin-Huxley neuron model [16] and its respective simplifications, e.g., FitzHugh-Nagumo model [11], Morris-Lecar model [31], Hindmarsh-Rose model [37], to completely theoretical models such as Wilson polynomial model [51] and Izhikevich model [20].

In addition to an external source, the change of concentration of ions in a neuron cell could also lead to the occurrence of electromagnetic induction. This phenomena is inspected in [29], where authors introduce the four-variable Hindmarsh-Rose neuron model with an additive variable used in order to obtain feedback memrisitve current, which directly depends on the variation of magnetic flow. The previously outlined work is further improved in [28], where the electrical neuronal activity mode transition is investigated by applying external electromagnetic radiation on the improved three-variable Hindmarsh-Rose neuron model. Furthermore, the effect of electromagnetic induction, described by the modulation of magnetic flux on the membrane potential of a neuron, realized using memristor coupling together with an additive phase noise imposed on the neuron in order to detect the dynamical response and phase transition mode, is investigated in [53]. Authors in [30] have carried out an extensive review of all relevant literature considering dynamics in a neuron and neuronal network, paying special attention to realization of a computational model under the effect of electromagnetic induction and/or radiation in order to better understand the electromagnetic effect in treating neurodegenerative diseases. The dynamics of the action potential of a neuron under the electromagnetic induction is shown to be greatly dependant on the environmental surrounding temperature in [27] using the extended induction-based Hodgkin-Huxley neuron model, similar to that used in this paper. The temperature influence is previously verified in the clinical study, where temperature effects are examined in rat hypothalamic tissue slices [59]. The action potential of a neuron largely depends on the stimulus itself, especially if the noise is present [33]. Recently, many studies have been carried out, where both the presence of noise and the electromagnetic induction is observed through dynamical analysis framework for a single neuron [24, 26, 50] and neural networks [14, 25, 56]. Oftentimes, realistic neurons hold complex anatomical structure, for instance, autapse connection to some internuncial neurons. The autaptic regulation of electrical activity modes in a neuron under the effect of electromagnetic induction is investigated in [57]. The complexity of a neuron can also be observed through its electrical properties – a neuron is a charged body where any changes in fluctuation of either magnetic flux or electric charge can cause field variation and thus the variation in electrical properties of a neuron. A novel neuron model, able to capture the effect of the total electromagnetic field, is developed and described by dimensionless dynamical system and is verified on analog circuit platform [52]. Another important factor, the energy, is investigated in [58], where authors analyze the role of the energy supply in brain metabolism and signal transmission by using Izhikevich neuron model in the presence of electromagnetic field. Ion channels conductivity is large impact factor on the overall electrical behaviour of a neuron as well [40, 41].

All previously outlined model variants of a single neuron and neuronal network have a common purpose – reliability and interpretability of the output where the greatest attention is usually paid to nonlinear dynamical analysis through bifurcation or phase graphs to determine the influence of various factors (radiation, induction, noise, temperature) on the dynamics of the action potential on the membrane and consequently to gain insight on the coding and information transfer, brain metabolism, potential treatments for neurodegenerative disorders, etc. However, a large impact of error, i.e. uncertainties, in parameter space and initial conditions is often neglected and all relevant papers published in the field of neural nonlinear dynamics and computational neuroscience, to the best of our knowledge, take the values of input parameters as constants. In this paper, by considering conductivity values of each ion channel in Hodgkin-Huxley neuron model as a random variable uniformly distributed around the expected value, the original deterministic system is recasted to stochastic system [54]. The expected values of ion channels conductivity are taken from the review study by Ma et al. in [30]. The stochastic collocation method is used as a method of choice for uncertainty quantification because of its non-intrusive nature – no requirements for intrinsic system formulation perturbation and manual interventions are needed. By computationally assessing the sensitivity of the action potential dynamics and the inter-spike interval (ISI) duration w.r.t the changes in the conductivity of ion channels of a neuron exposed to the electromagnetic induction, experimental procedures with magnetic fields, such as medical treatments of neurodegenerative diseases with transcranial

magnetic stimulation or deep stimulation [2], will be possible to adapt to different individuals in various environmental conditions.

The outline of the paper is as follows: the formulation of the extended Hudgkin-Huxley neuron model is given in Section 2, numerical simulations and results of bifurcation analysis for two different types of the external neuronal stimulus are given in Section 3, the sensitivity analysis of a neuron model electrophysiology by considering ion channels conductivity as random variables is given in Section 4, finally, concluding remarks are outlined in Section 5.

2 Formulation

The model of choice in this study is Hodgkin-Huxley neuron model [16], originally described as a set of four coupled non-linear ordinary differential equations. The greatest significance of Hodgkin-Huxley neuron model is that it is bio-physically meaningful (describing the dynamics of membrane potential under the influence of some external stimulus, the dynamics of ionic currents, synaptic integration, etc.), measurable and readily available for bifurcation analysis [21]. Although Hodgkin-Huxley neuron model is prohibitive and computationally expensive, which additionally causes implementation difficulties and extended simulation time, since the focus of the study is on the electromagnetic effect on a single neuron, rather than on a neural network, these shortcomings can be overlooked. In order to capture the electromagnetic induction in a neuron cell governed by the Faraday's law, an additive variable in a membrane potential equation of Hodgkin-Huxley model is introduced. This variable further extends the original model with an additional equation describing the change in the magnetic flux, φ. Hodgkin-Huxley neuron model is then given in the following form [27]:

$$\begin{aligned}\frac{dV_m}{dt} = \frac{1}{C_m}\Big(&\bar{g}_K n^4 (V_m - E_K) + \bar{g}_{Na} m^4 h (V_m - E_{Na}) \\ &+ g_L (V_m - E_L) + I_{ext} - k\rho(\varphi) V_m\Big)\end{aligned} \tag{1}$$

$$\frac{dy}{dt} = \alpha_y (1-y) - \beta_y y, \qquad y = (n, m, h) \tag{2}$$

$$\frac{d\varphi}{dt} = k_1 V_m - k_2 \varphi \tag{3}$$

Equation (1) describes the change of the membrane potential, V_m, in time, where C_m stands for the lipid bi-layer capacitance and $\bar{g}_K$, $\bar{g}_{Na}$ and $\bar{g}_L$ are maximum values of potassium, sodium and leakage ion channel conductivity, respectively. E_K, E_{Na} and E_L are associated reversal potentials for potassium, sodium and leakage ion channel, respectively. I_{ext} represents the external neuro-stimulus by means of the electric current source.

The dynamics of gating variables, denoted as y, is outlined in (2), where α_y and β_y represent an ion channel gate's opening and closing rate, respectively. Each gating variable, $y = n$ for the potassium ion channel, $y = m$ for the sodium ion channel or $y = h$ for the leakage ion channel, has its activation and inactivation steady state represented by the Boltzmann equation as a function of the membrane potential, V_m, and the environmental temperature, T, as follows:

$$\alpha_n(V_m, T) = \frac{0.01\phi(T)(10 - V_m)}{e^{(10-V_m)/10} - 1} \tag{4}$$

$$\beta_n(V_m, T) = 0.125\phi(T) e^{-V_m/80} \tag{5}$$

$$\alpha_m(V_m, T) = \frac{0.1\phi(T)(25 - V_m)}{e^{(25-V_m)/10} - 1} \tag{6}$$

$$\beta_m(V_m, T) = 4\phi(T) e^{-V_m/18} \tag{7}$$

$$\alpha_h(V_m, T) = 0.07\phi(T) e^{-V_m/20} \tag{8}$$

$$\beta_h(V_m, T) = \frac{\phi(T)}{e^{(30-V_m)/10} + 1} \tag{9}$$

where the function governing the environmental temperature is defined in the following manner:

$$\phi(T) = 3^{(T-6.3)/10} \tag{10}$$

Arising from the Faraday's law in the Maxwell's framework, the presence of a time-varying magnetic field across an electrical conductor will induce a spatially varying non-conservative electric field. Since the neuron cell is electrically short when represented by a transmission line model, which Hudgkin-Huxley neuron model intrinsically is, only temporal, rather than spatial variability, needs to be observed. Thus, the feedback current of magnetic flux could be realized by placing the memristor in parallel in Hodgkin-Huxley neuron model equivalent electric circuit, Fig. 1.

Memristor (abbreviation of memory resistor) is a non-linear resistor with memory introduced by Chua in [5] as the forth fundamental electric circuit element that outlines the missing link between the charge, $q(t) = \int_{-\infty}^{t} i(\tau) d\tau$, and the magnetic flux, $\varphi(t) = \int_{-\infty}^{t} v(\tau) d\tau$:

$$d\varphi = M(q) dq \tag{11}$$

where $M(q)$ is the memristance (abbrevation of memristor's resistance) measured in Ω. Memristor, memristive systems and possible applications are further elaborated in [6]. The first physical realization of the memristor is achieved in the work by Strukov et al. [48], by constructing a nanoscale-thin film device which is equivalent to a time-dependant resistor whose value at time t is linearly proportional to the amount of charge that has passed through it before. The memristor device can be modelled as serially connected doped resistor, R_{on}, and undoped resistor, R_{off}, and its iv characteristic is given in a review paper by Joglekar et al. [22] as follows:

$$i(t) = \frac{v(t)}{M(q(t))} = \frac{v(t)}{R0\sqrt{1 - 2\eta\Delta R\varphi(t)/(Q_0 R_0^2)}} \tag{12}$$

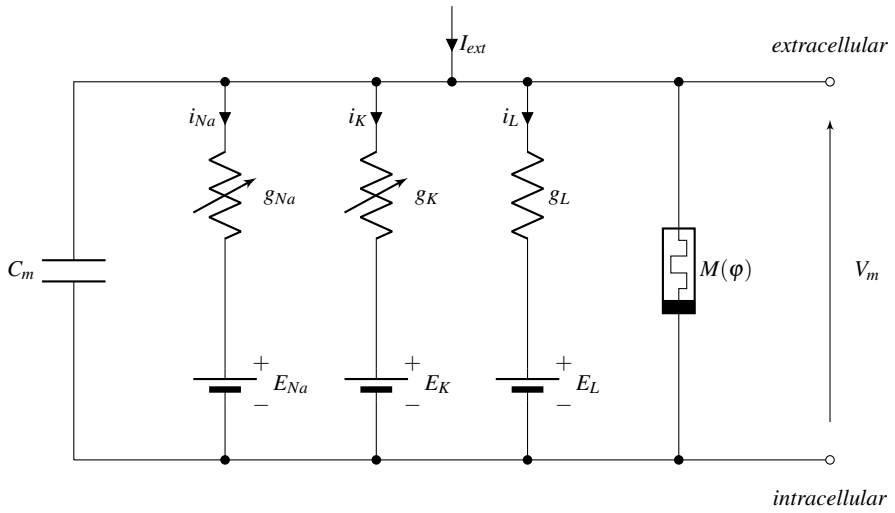

Fig. 1 Hodgkin-Huxley neuron model equivalent electrical circuit [16] with the magnetic flux-controlled memristor, used to bridge the gap between the magnetic flux and the membrane potential and to enable the trans-membrane feedback current flow.

R_0 stands for the total resistance at time $t = 0$ and is formulated as:

$$R_0 = \frac{w_0}{D} R_{on} + \left(1 - \frac{w_0}{D}\right) R_{off} \tag{13}$$

where w_0 is the initial length of the doped region and D is the total length of the memristor. The polarity of the memristor can be either $\eta = +1$, when the dopant drift expands the doped region, or $\eta = -1$, when the contraction of the doped region occurs. Furthermore, ΔR is the difference in resistance of two regions:

$$\Delta R = R_{off} - R_{on} \tag{14}$$

Finally, Q_0 is the total charge value that is required to pass through the memristor for the dopant boundary to move through the entire length of the memristor, D:

$$Q_0 = \frac{D^2}{\mu^2 R_{on}} \tag{15}$$

where the mobility of a dopant is represented as μ.

Equation (12) describes the memristor as a purely dissipative electric circuit element in a sense that it does not store, supply or transmit energy. However, in order to simplify the numerical implementation of the memristor, distance ourselves from the physical details of the memristor realization itself, and ensure seamless simulation process, we assume memristor as a flux-controlled smooth continuous cubic monotone-increasing non-linear function as given in Bao et al. [1]:

$$q(\varphi) = a\phi + b\phi^3 \tag{16}$$

where a and b are arbitrary positive parameters. The memductance (abbrevation of memristor's conductance) measured in S, is defined as:

$$\rho(\varphi) = \frac{dq(\varphi)}{d\varphi} = a + 3b\varphi^2 \tag{17}$$

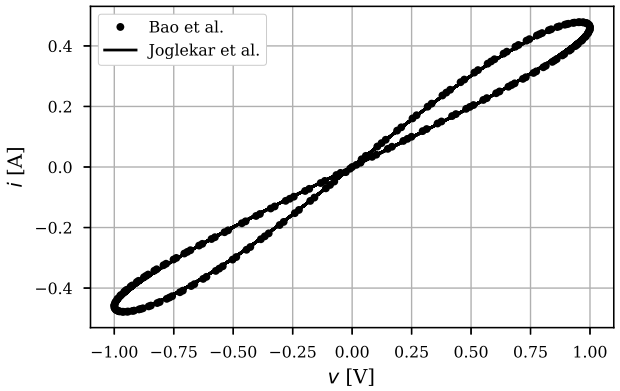

Fig. 2 Visual representation of the *iv* characteristic compatibility between the non-linear polynomial approximatin of the memristor given in Bao et al. [1] and the actual memristor device realization [22] given in Joglekar et al.

and is embedded in (1) after being scaled by factor k that describes the suppression modulation on the membrane potential [29]. The product term $k\rho(\varphi)V_m$ is the additive induction current posed on the neuron membrane. Parameters a and b of a non-linear polynomial approximation of the memristor are chosen to be 0.4 and 0.02 as in [27]. To physically justify the choice of a and b, parameters in 12 are fitted via Nelder-Mead simplex algorithm [32] and the compatibility between the non-linear polynomial approximation of the memristor and the actual *iv* characteristics of the memristor is shown in Fig. 2. The full list of free parameters, the details of the fitting procedure and the implementation nuances are elaborated in Appendix A.

Finally, equation (3) in Hodgkin-Huxley neuron model outlines the dynamics of the magnetic flux, φ, where the term $k_1 V_m$ describes the membrane potential-induced flux changes and the term $k_2\varphi$ describes the flux leakage [28].

3 Numerical simulations

Expected maximum values of ion channel conductivity are set as in [7] as follows: $\bar{g}_K = 36.0$ mS/cm^2, $\bar{g}_{Na} = 120.0$ mS/cm^2 and $\bar{g}_L = 0.3$ mS/cm^2, with the coefficient of variation (CV) of 5, 10 and 20 per cent, respectively. The rest of the parameters and the initial condition setup of Hodgkin-Huxley neuron model are given in Table 1.

Numerical solution for all calculations in the study of (1)-(3) is carried out by using the MATLAB® implementation of nonstiff differential equation solver based on the fourth order Runge-Kutta integration method [42].

The simulation of an action potential dynamics is carried out within two different electrical modes in the following two subsections. The first mode, outlined in Subsection 3.1, is so-called tonic spiking electrical mode [21], where the action potential, represented as a time series of discrete, nearly identical membrane potential spikes, encode information and carry it throughout a neuron's cell. The distribution of ISIs is close to an exponential distribution [8], where the total entropy is found to be ~ 2.0. On the other hand, the second mode, outlined in Subsection 3.2, is so-called tonic bursting electrical mode [21], where periods of rapid action potential spiking (bursting) are followed by quiescent periods typically of longer duration than the mean ISI. Bursting usually occurs either depending on the type of a neuron and its intrinsic configuration or depending on the type of the stimulus. This study examines the case of the latter – bursting is the response of a neuron w.r.t. the external noisy stimulus current.

3.1 Tonic spiking electrical mode

The tonic spiking behaviour is achieved by using the external stimulus direct current (dc) set to $I_{ext}(t) = 10$ µA/cm^2 for a complete simulation duration of $\Delta t_{sim} = 1500$ ms. Induction coefficient, k, is set to a constant value of $k = 0.1$, while the parameter in the potential-based change of the magnetic flux term in (3) is set to $k_1 = 0.001$ and the parameter in the magnetic flux leakage term in (3) is set to $k_2 = 0.01$. This kind of tonic spiking behaviour represents the optimal behaviour of a neuron exposed to the electromagnetic induction effect, where optimality is viewed as the ability to transfer maximum information, expressed through the entropy measure. Even though, in computational neuroscience literature, entropy is expressed in different forms for a variety of measured data, more details on the topic can be found elsewhere, e.g., [47], we assume the entropy definition as in the original work by Shannon [43]:

$$H = -\sum_{i}^{n} p(\mathrm{x}_i) \log\big(p(\mathrm{x}_i)\big) \tag{18}$$

where observable x_i is the i-th ISI in the simulation. For the previously outlined simulation configuration, action potential dynamics along with the probability mass function of ISIs, captured post-simulation, are shown in Fig. 3.

The effect of the electromagnetic induction is investigated via bifurcation analysis where the induction coefficient, k, is taken as the bifurcation parameter. Bifurcation analysis consisted of a repeated simulation of a fixed-configuration Hodgkin-Huxley neuron model at a constant temperature of $T = 10$ °C for the induction coefficient ranging from 0 to 2. Instead of displaying all ISIs, the expected value of ISI, $\langle \mathrm{ISI} \rangle$, is evaluated. Furthermore, by using a stochastic collocation method, details on the method available elsewhere, e.g., in [55], the output uncertainty by means of 95 per cent confidence interval is determined. The uncertainty comes from the fact that we observe the conductance of each ion channel in Hodgkin-Huxley neuron model as a random variable uniformly distributed around its expected value. The stochastic analysis is performed by using 3, 5, 7 and 9 collocation points in each stochastic dimension, thus leading to the total of 27, 125, 343 and 729 deterministic simulations respectively. Collocation level is changed from 3 to 9 in order to test the convergence of the stochastic collocation method and, as shown in Fig. 4, the convergence is satisfying for 5 collocation points, which is used for further stochastic analysis. Therefore, a total of 125 deterministic simulations is performed in order to carry out the uncertainty quantification and sensitivity analysis by means of stochastic collocation method.

Mean ISI over range of $k \in [0,2]$ in simulation duration of $\Delta t_{sim} = 300$ ms using 5 collocation points for CV = 5, 10 and 20 per cent is shown in Fig. 5, Fig. 6, and Fig. 7, respectively. All three figures, 5 - 7, show the same exact behavior of a neuron exposed to the effect of electromagnetic induction: an increase of the induction coefficient leads to a decrease in neuronal activity with the notable values of k in range from $k \sim 1$ to $k \sim 1.5$, in which the greatest influence of the uncertainty of ion channels conductivity is detectable, after which the transition from a spiking state to a quiescent state occurs.

3.2 Tonic bursting electrical mode

The tonic spiking behaviour is achieved by using the noisy periodic current set to $I_{ext}(t) = 10\sin(\omega t) + \text{w.n. µA/cm}^2$ as an external stimulus of a neuron for a complete simulation duration of $\Delta t_{sim} = 1500$ ms. The angular frequency, ω, is set to $\omega = 100/\Delta t_{sim}$ Hz, and w.n. stands for white noise. Since the input is characterized by a large signal-to-noise ratio, compared to the ideal input for the tonic spiking electrical mode, the distribution of ISIs is less like an exponential distribution with, as expected, lower value of the entropy. All parameters of Hodgkin-Huxley neuron model along with induction parameters are set as in the previous simulation

Table 1 Hodgkin-Huxley neuron model setup

Parameters		
Name or description	Label	Value
lipid bi-layer conductance	C_m	$1.0\ \mu\text{F}/\text{cm}^2$
potassium channel reversal potential	E_K	-77.0 mV
sodium channel reversal potential	E_{Na}	50.0 mV
leakage channel reversal potential	E_L	-54.387 mV
environmental temperature	T	6.3 °C
Initial conditions		
Name or description	Label	Value
membrane potential value at $t = 0$	$V_{m,0}$	-65.0 mV
magnetic flux value at $t = 0$	ϕ_0	0.1 mV s
potassium channel gating variable value at $t = 0$	m_0	$\frac{\alpha_m(V_{m,0},T)}{\alpha_m(V_{m,0},T)+\beta_m(V_{m,0},T)}$
sodium channel gating variable value at $t = 0$	n_0	$\frac{\alpha_n(V_{m,0},T)}{\alpha_n(V_{m,0},T)+\beta_n(V_{m,0},T)}$
	h_0	$\frac{\alpha_h(V_{m,0},T)}{\alpha_h(V_{m,0},T)+\beta_h(V_{m,0},T)}$

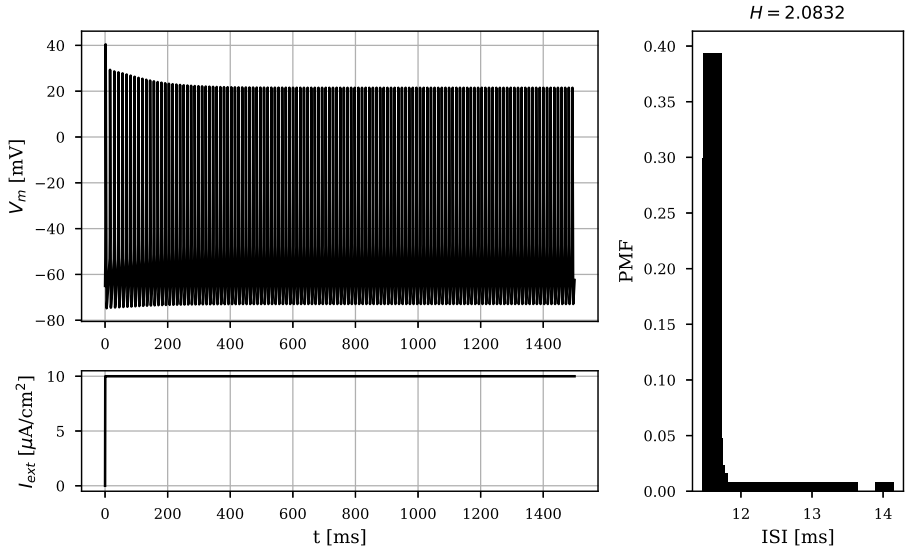

Fig. 3 Action potential dynamics, $V_m(t)$, shown in the top left subfigure, for the case of the direct current external stimulus, $I_{ext}(t)$, shown in the bottom left subfigure. Subfigure on the right depicts the probability density histogram (probability mass function) of ISIs, visually resembling an exponential distribution. Entropy amounts to $H = 2.0832$ for the number of bins determined via the Freedman-Diaconis rule [12].

in which the tonic spiking is achieved. The simulation is depicted in Fig. 8.

Similar to the previous subsection, bifurcation analysis is performed in order to investigate the effect of electromagnetic induction on a neuron, in this case, stimulated by a noisy periodic current. In this simulation, environmental temperature is set to $T = 6.3$ °C. Induction coefficient, ranging from 0 to 5 is again set as the bifurcation parameter. Remaining parameters are not changed and the simulation is performed for 3, 5, 7 and 9 collocation points, respectively. Convergence graph is shown in Fig. 9.

Mean ISI over range of $k \in [0,5]$ in simulation duration of $\Delta t_{sim} = 300$ ms using 5 collocation points for CV = 5, 10 and 20 is shown in Fig. 10, Fig. 11, and Fig. 12, respectively.

Again, all three figures, 10 - 12, show the exact behavior of a neuron exposed to the effect of electromagnetic induction: an increase of the induction coefficient leads to a decrease in neuronal activity. Here, a neuron undergoes two activity transitions. The first transition occurs at $k \sim 0.5$, where a bursting state remains unchanged up until $k \sim 0.88$. The second transition occurs after a sharp decrease of expected ISI when the neuron passes into a quiscent state at $k \sim 1.5$.

4 Sensitivity analysis

Sensitivity analysis ranks input parameters from the most to the least significant ones with respect to the impact their

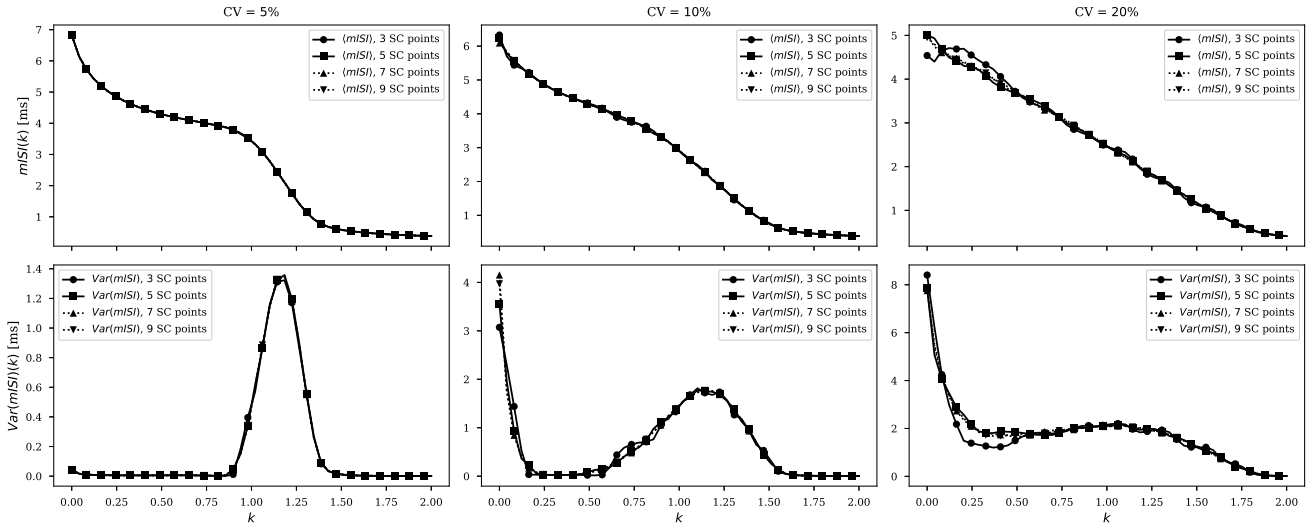

Fig. 4 Convergence graph for the stochastic collocation method applied on bifurcation analysis of Hodgkin-Huxley neuron model for $k \in [0,2]$. The convergence of the mean value for ISI is depicted in the first row, while the convergence for the variance is depicted in the second row for 4 levels of accuracy: 3, 5, 7 and 9 collocation points respectively. Each column depicts simulations for a different coefficient of variation, CV = 5, 10 and 20 per cent.

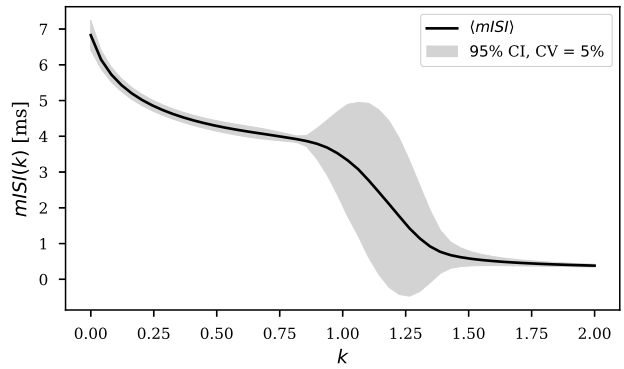

Fig. 5 Mean ISI as a function of k inside 95 per cent confidence interval obtained via 5 collocation points and a coefficient of variation CV = 0.05.

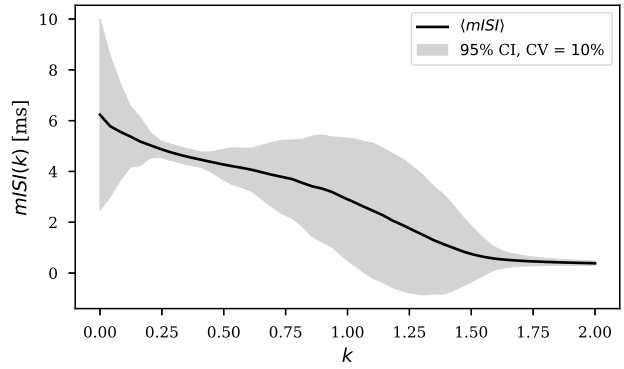

Fig. 6 Mean ISI as a function of k inside 95 per cent confidence interval obtained via 5 collocation points and a coefficient of variation CV = 0.1.

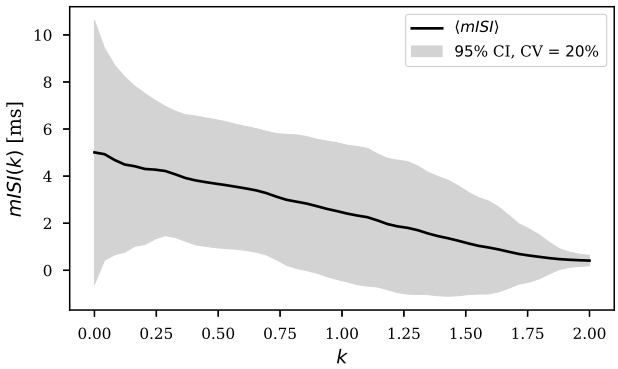

Fig. 7 Mean ISI as a function of k inside 95 per cent confidence interval obtained via 5 collocation points and a coefficient of variation CV = 0.2.

variability has on the total variance of the output of interest. In this work, sensitivity analysis is carried out according to a so-called analyis of variance (ANOVA) principle [38]. ANOVA is based on a Hoeffding function decomposition and computation of Sobol indices [46]. Namely, the total variance due to the variability of all random input parameters is decomposed into terms corresponding to variances due to variability present in all possible subsets of random input parameters.

ANOVA sensitivity analysis results are presented in form of the first and higher order sensitivity indices. The sensitivity analysis in this work is 3-dimensional from stochastic point of view since random input parameters are: $\bar{g}_{Na}$, $\bar{g}_K$ and $\bar{g}_L$. Thus, there are three first order sensitivity indices, $S_1(\hat{g}_{Na})$, $S_1(\bar{g}_K)$ and $S_1(\bar{g}_L)$, each corresponding to the impact of $\bar{g}_{Na}$, $\bar{g}_K$ and $\bar{g}_L$. Higher order sensitivity indices reflect the impact

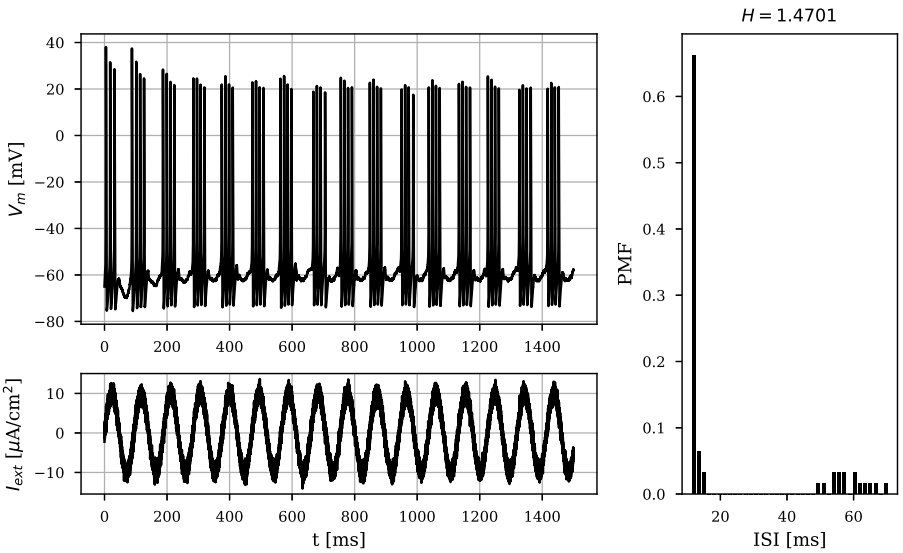

Fig. 8 Action potential dynamics, $V_m(t)$, shown in the top left subfigure, for the case of the direct current external stimulus, $I_{ext}(t)$, shown in the bottom left subfigure. Subfigure on the right depicts the probability density histogram (probability mass function) of ISIs. Entropy amounts to $H = 1.4701$ for the number of bins determined via the Freedman-Diaconis rule [12].

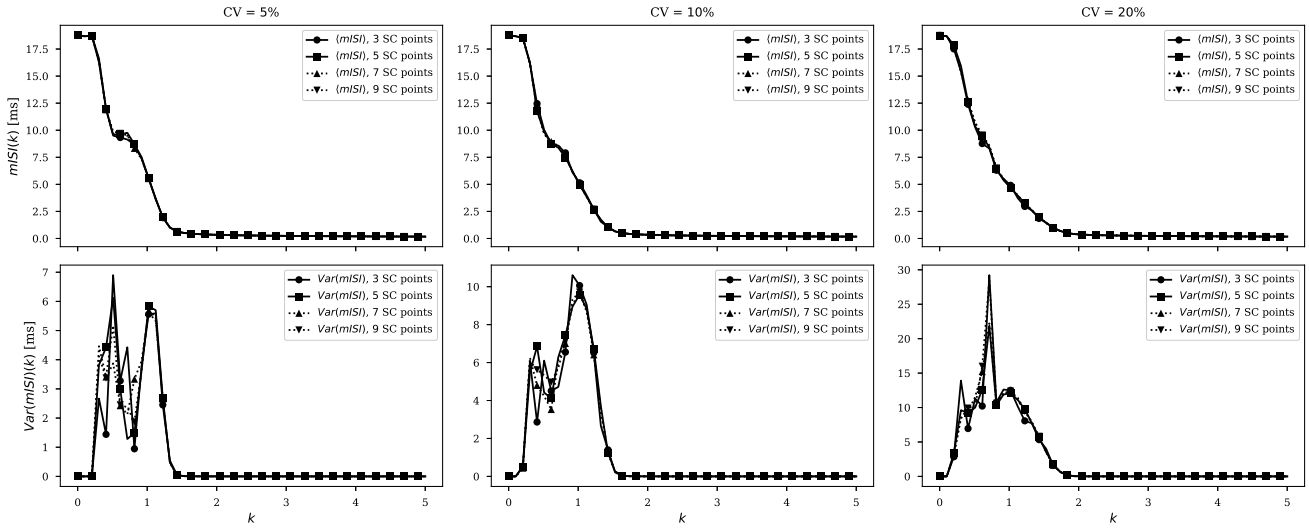

Fig. 9 Convergence graph for the stochastic collocation method applied on bifurcation analysis of Hodgkin-Huxley neuron model for $k \in [0,5]$. The convergence of the mean value for ISI is depicted in the first row, while the convergence for the variance is depicted in the second row for 4 levels of accuracy: 3, 5, 7 and 9 collocation points respectively. Each column depicts simulations for a different coefficient of variation, CV = 5, 10 and 20 per cent.

of mutual interactions of input parameters. There are three second order sensitivity indices, $S_2(\bar{g}_{Na}, \bar{g}_K)$, $S_2(\bar{g}_{Na}, \bar{g}_L)$ and $S_2(\bar{g}_K, \bar{g}_L)$, reflecting the impact of the interaction between the associated conductivity subsets. Higher stochastic dimensions yield even higher order sensitivity indices because number of subsets corresponding to mutual interactions of input parameters grows.

If stochastic dimension is too large, a total effect sensitivity index may be computed in order to avoid the computation of higher order sensitivity indices to ultimately reduce the computation time. The total effect index measures the contribution to the output variance of a single input parameter including all variances caused by its interactions, of any order, with any other input variables. E.g., the total effect index $S_T(\bar{g}_{Na})$ measures the total effect sensitivity that $\bar{g}_{Na}$ has, together with its interaction to $\bar{g}_K$ and $\bar{g}_L$, on the mean ISI distribution over k. If the first order and total effect indices have virtually the same value, the mutual interactions have a negligible impact on the variation of the output value.

Sensitivity indices are shown in Fig. 13 for the case of tonic spiking electrical mode, and in Fig. 14 for the case of tonic bursting electrical mode. Both modes are exposed to the

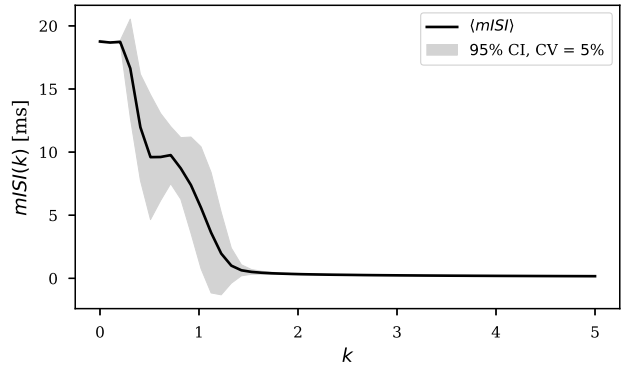

Fig. 10 Mean ISI as a function of k inside 95 per cent confidence interval obtained via 5 collocation points and a coefficient of variation $\mathrm{CV} = 0.05$.

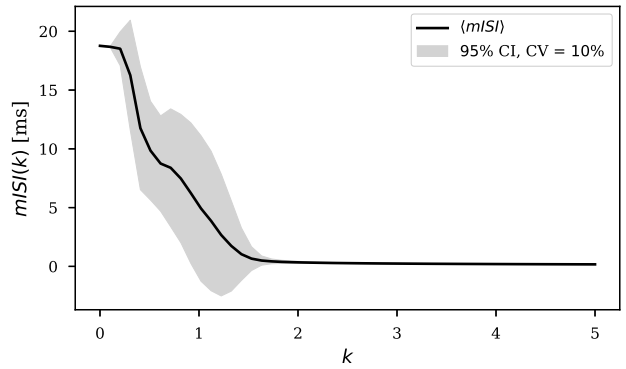

Fig. 11 Mean ISI as a function of k inside 95 per cent confidence interval obtained via 5 collocation points and a coefficient of variation $\mathrm{CV} = 0.1$.

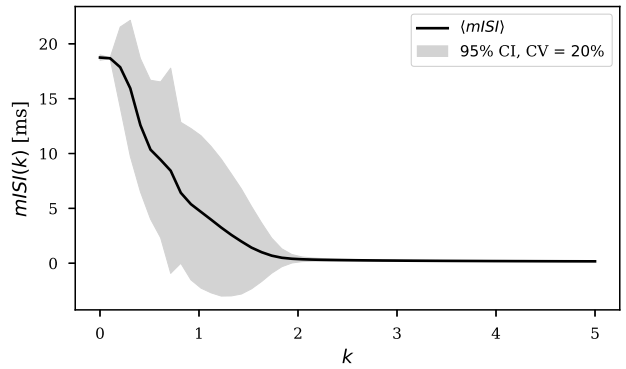

Fig. 12 Mean ISI as a function of k inside 95 per cent confidence interval obtained via 5 collocation points and a coefficient of variation $\mathrm{CV} = 0.2$.

electromagnetic induction effect where induction coefficient is in range $[0,2]$ and $[0,5]$ for the tonic spiking and tonic bursting electrical mode, respectively.

Interestingly, for $\mathrm{CV} = 5$ and $\mathrm{CV} = 10$ per cent, the mean ISI hard drop in the critical range of k values for the tonic spiking electrical mode is affected by the variability in the interaction of the sodium and potassium ion channels, and the leakage channel variability exerts practically no impact. For $\mathrm{CV} = 20$ per cent, the output, that is mean ISI over k in range $[0,2]$, is most sensitive w.r.t. the variability in sodium ion channel from the starting point of the critical induction coefficient range, $k \sim 0.75$.

For all CVs, the variability of the sodium channel beginning at $k \sim 1$ onward has the largest impact on the mean ISI, for the tonic bursting electrical mode. For $k < 1$, the first order and the total effect sensitivity indices revolve around similar values and the significance of the impact is difficult to discern. Both sodium and potassium ion channel, as well as the respective second order combinations, achieve quite similar behavior and influence on the output.

5 Conclusion

An extended variant of Hodgkin-Huxley neuron model under the electromagnetic induction is developed. In the presence of an induced electric field governed by the Faraday's law of induction, associated electrical feedback current is embedded in the model using a theoretical model of a flux-controlled memristor. Both numerical simulation and stochastic sensitivity analysis are performed in order to assess the influence of the uncertainties on the output, where the output has been represented as the dependence of the mean inter-spike interval for various induction coefficient values, which ultimately indicate the strength of the magnetic field to which the isolated cortex neuron has been exposed. The uncertainty on the output of the model arises from the propagated uncertainties of the conductivity of ion channels, often neglected in the literature. Additionally, stochastic sensitivity analysis is performed, where it is shown that the output depends mostly on the interaction of variability in the conductivity of sodium and potassium ion channel (second order sensitivity). Insights gained from this paper can greatly contribute to the development of experimental applications of induction for therapeutic purposes, especially in medical treatments of neurodegenerative disorders.

6 Declarations

6.1 Fundings

This research has been funded by DATACROSS project of The Centre of Research Excellence for Data Science and Advanced Cooperative Systems (CRE ACROSS-DataScience).

6.2 Conflict of interest

The authors declare that they have no conflict of interest.

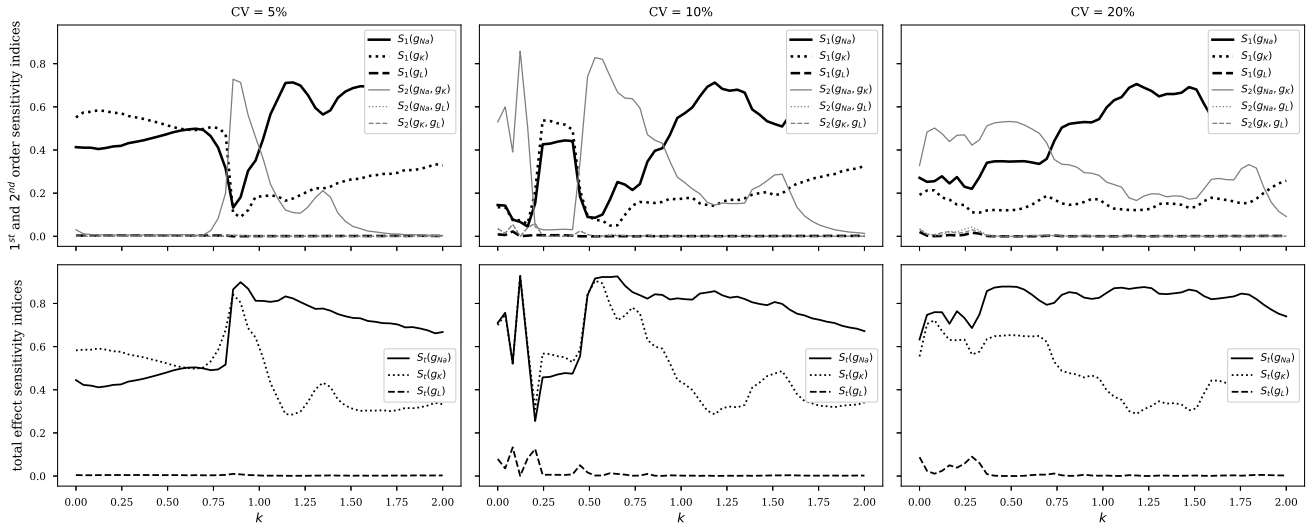

Fig. 13 Variance-based sensitivity analysis for Hodgkin-Huxley neuron model under the influence of the electromagnetic induction. External neuronal stimulus for the case visualized in this figure is constant dc current. Upper row holds the first and the second order sensitivity indices of the output given $\bar{g}_{Na}$, $\bar{g}_K$ and $\bar{g}_L$ respectively, for the case of 5 collocation points. Lower row holds the total effect sensitivity indices of the output. Each column shows simulations for a different coefficient of variation.

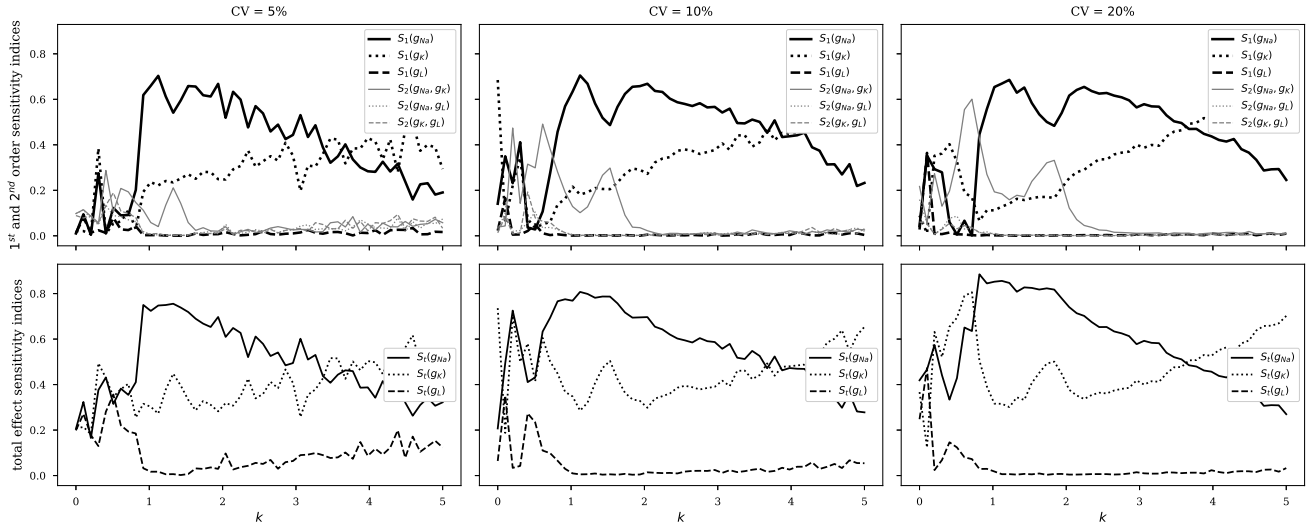

Fig. 14 Variance-based sensitivity analysis for Hodgkin-Huxley neuron model under the influence of electromagnetic induction. External neuronal stimulus for the case visualized in this figure is noisy periodic current. Upper row holds the first and the second order sensitivity indices of the output given $\bar{g}_{Na}$, $\bar{g}_K$ and $\bar{g}_L$ respectively, for the case of 5 collocation points. Lower row holds the total effect sensitivity indices of the output. Each column shows simulations for a different coefficient of variation.

6.3 Code availability

To enable seamless reproduction and re-implementation of results presented in this study, thereby to support the Open Science movement, the entire associated code-base is available on the first author's GitHub:

`https://github.com/antelk/em-hodgkin-huxley`

6.4 Availability of data and material

`https://github.com/antelk/em-hodgkin-huxley/tree/main/src/output`

A Fitting the *iv* characteristic of the memristor

To physically justify the choice of a and b in (17), parameters D, μ and R_{on} are set to be fitted. Parameter R_{off} is assumed to be 20 times greater then free parameter R_{on} and parameter w is assumed to be 0.2 times the value of the parameter D. The physical memristor's polarity is assumed to be $\eta = -1$. The formulation for the memristance of the

physical memristor is defined as follows:

$$M(q(t)) = R_0\sqrt{q - 2\eta\Delta R\phi(t)/(Q_0R_0^2)} \tag{A.1}$$

where R_0, ΔR and Q_0 are given in (13), (14) and (15), respectively. Loss function is defined as the mean square error between the memristance of the actual physical memristor given in (A.1) and the memristance of the non-linear approximation of the memristor given as the reciprocal of the expression in (17) for various time-dependent charge values. The optimization is performed using the Python scientific module SciPy [49] or, more precisely, its implementation of the Nelder-Mead iterative minimization method [13]. The convergence graph is shown in Fig. 2, where free parameters took on the following values:

$R_{on} = 1.589 \cdot 10^{-1}\ \Omega$
$\mu = 6.237 \cdot 10^{-14}\ \mathrm{m}^2/\mathrm{Vs}$
$D = 1.698 \cdot 10^{-7}\ \mathrm{m}$

Acknowledgements This research has been funded by DATACROSS project of The Centre of Research Excellence for Data Science and Advanced Cooperative Systems (CRE ACROSS-DataScience).

References

1. Bao, B., Liu, Z., Xu, J.: Steady periodic memristor oscillator with transient chaotic behaviours. Electronics Letters **46** (2010). DOI 10.1049/el.2010.3114
2. Barker, A., Jalinous, R., Freeston, I.: Non-invasive magnetic stimulation of human motor cortex. The Lancet **325** (1985). DOI 10.1016/S0140-6736(85)92413-4
3. Barker, A.T., Freeston, I.L., Jalinous, R., Jarratt, J.A.: Magnetic stimulation of the human brain and peripheral nervous system: an introduction and the results of an initial clinical evaluation. Neurosurgery **20**(1) (1987). DOI 10.1097/00006123-198701000-00024
4. Capelli, E., Torrisi, F., Venturini, L., Granato, M., Fassina, L., Lupo, G.F.D., Ricevuti, G.: Low-frequency pulsed electromagnetic field is able to modulate miRNAs in an experimental cell model of Alzheimer's disease. Journal of Healthcare Engineering (2017). DOI 10.1155/2017/2530270
5. Chua, L.O.: Memristor – the missing circuit element. IEEE Transactions on Circuit Theory **18**(5) (1971). DOI 10.1109/TCT.1971.1083337
6. Chua, L.O., Kang, S.M.: Memristive devices and systems. Proceedings of the IEEE **64**(2) (1976). DOI 10.1109/PROC.1976.10092
7. Clay, J.R.: Excitability of the squid giant axon revisited. Journal of Neurophysiology **80**(2) (1998). DOI 10.1152/jn.1998.80.2.903
8. Dorval, A.: Probability distributions of the logarithm of inter-spike intervals yield accurate entropy estimates for small datasets. Journal of neuroscience methods **173** (2008). DOI 10.1016/j.jneumeth.2008.05.013
9. Ermentrout, G.B., Kopell, N.: Parabolic bursting in an excitable system coupled with a slow oscillation. SIAM Journal on Applied Mathematics **46**(2) (1986). DOI 10.1137/0146017
10. Fisher, R., Salanova, V., Witt, T., Worth, R., Henry, T., Gross, R., Oommen, K., Osorio, I., Nazzaro, J., Labar, D., Kaplitt, M., Sperling, M., Sandok, E., Neal, J., Handforth, A., Stern, J., DeSalles, A., Chung, S., Shetter, A., Bergen, D., Bakay, R., Henderson, J., French, J., Baltuch, G., Rosenfeld, W., Youkilis, A., Marks, W., Garcia, P., Barbaro, N., Fountain, N., Bazil, C., Goodman, R., McKhann, G., Babu Krishnamurthy, K., Papavassiliou, S., Epstein, C., Pollard, J., Tonder, L., Grebin, J., Coffey, R., Graves, N., the SANTE Study Group: Electrical stimulation of the anterior nucleus of thalamus for treatment of refractory epilepsy. Epilepsia **51**(5) (2010). DOI https://doi.org/10.1111/j.1528-1167.2010.02536.x
11. FitzHugh, R.: Impulses and physiological states in theoretical models of nerve membrane. Biophysical Journal **1**(6) (1961). DOI 10.1016/S0006-3495(61)86902-6
12. Freedman, D., Diaconis, P.: On the histogram as a density estimator: L2 theory. Zeitschrift für Wahrscheinlichkeitstheorie und Verwandte Gebiete **57**(2) (1981). DOI 10.1007/BF01025868
13. Gao, F., Han, L.: Implementing the Nelder-Mead simplex algorithm with adaptive parameters. Computational Optimization and Applications **51** (2012). DOI 10.1007/s10589-010-9329-3
14. Ge, M., Lu, L., Xu, Y., Mamatimin, R., Pei, Q., Jia, Y.: Vibrational mono-/bi-resonance and wave propagation in FitzHugh–Nagumo neural systems under electromagnetic induction. Chaos, Solitons & Fractals **133** (2020). DOI 10.1016/j.chaos.2020.109645
15. Gerstner, W., Kistler, W.M., Naud, R., Paninski, L.: Neuronal dynamics: From single neurons to networks and models of cognition. Cambridge University Press (2014). DOI 10.1017/CBO9781107447615
16. Hodgkin, A.L., Huxley, A.F.: A quantitative description of membrane current and its application to conduction and excitation in nerve. Bulletin of Mathematical Biology **52**(1) (1990). DOI 10.1016/S0092-8240(05)80004-7
17. ICNIRP: Guidelines for limiting exposure to time-varying electric and magnetic fields (1 Hz to 100 kHz). Health Physics **99**(6) (2010). DOI 10.1097/HP.0b013e3181f06c86
18. ICNIRP: Guidelines for limiting exposure to electromagnetic fields (100 kHz to 300 GHz). Health Physics **118** (2020). DOI 10.1097/HP.0000000000001210
19. Izhikevich, E.M.: Resonate-and-fire neurons. Neural Networks **14**(6) (2001). DOI 10.1016/S0893-6080(01)00078-8
20. Izhikevich, E.M.: Simple model of spiking neurons. IEEE Transactions on Neural Networks **14**(6) (2003). DOI 10.1109/TNN.2003.820440
21. Izhikevich, E.M.: Which model to use for cortical spiking neurons? IEEE Transactions on Neural Networks **15**(5) (2004). DOI 10.1109/TNN.2004.832719
22. Joglekar, Y.N., Wolf, S.J.: The elusive memristor: properties of basic electrical circuits. European Journal of Physics **30** (2009). DOI 10.1088/0143-0807/30/4/001
23. Lianghui, Q., Lin, D., Haiwei, H., Cao, Z., Zichen, D.: Pattern control of external electromagnetic stimulation to neuronal networks. Nonlinear Dynamics **102** (2020). DOI 10.1007/s11071-020-06076-6
24. Liu, Y., Ma, J., Xu, Y., Jia, Y.: Electrical mode transition of hybrid neuronal model induced by external stimulus and electromagnetic induction. International Journal of Bifurcation and Chaos **29**(11) (2019). DOI 10.1142/S0218127419501566
25. Lu, L., Jia, Y., Ge, M., Xu, Y., Li, A.: Inverse stochastic resonance in Hodgkin–Huxley neural system driven by Gaussian and non-Gaussian colored noises. Nonlinear Dynamics **100** (2020). DOI 10.1007/s11071-020-05492-y
26. Lu, L., Jia, Y., Liu, W., Yang, L.: Mixed stimulus-induced mode selection in neural activity driven by high and low frequency current under electromagnetic radiation. Complexity **2017** (2017). DOI 10.1155/2017/7628537
27. Lu, L., Kirunda, J.B., Xu, Y., Kang, W., Ye, R., Zhan, X., Jia, Y.: Effects of temperature and electromagnetic induction on action potential of Hodgkin–Huxley model. The European Physical Journal Special Topics **227** (2018). DOI 10.1140/epjst/e2018-700140-1
28. Lv, M., Ma, J.: Multiple modes of electrical activities in a new neuron model under electromagnetic radiation. Neurocomputing **205** (2016). DOI 10.1016/j.neucom.2016.05.004
29. Lv, M., Wang, C., Guodong, R., Song, X.: Model of electrical activity in a neuron under magnetic flow effect. Nonlinear Dynamics **85** (2016). DOI 10.1007/s11071-016-2773-6
30. Ma, J., Jun, T.: A review for dynamics in neuron and neuronal network. Nonlinear Dynamics **89** (2017). DOI 10.1007/s11071-017-3565-3

31. Morris, C., Lecar, H.: Voltage oscillations in the barnacle giant muscle fiber. Biophysical Journal **35**(1) (1981). DOI 10.1016/S0006-3495(81)84782-0
32. Nelder, J., Mead, R.: A simplex method for function minimization. The Computer Journal **7** (1965). DOI 10.1093/comjnl/7.4.308
33. Ozer, M., Ekmekci, N.H.: Effect of channel noise on the time-course of recovery from inactivation of sodium channels. Physics Letters A **338**(2) (2005). DOI 10.1016/j.physleta.2005.02.039
34. Park, H.J., Bonmassar, G., Kaltenbach, J.A., Machado, A.G., Manzoor, N.F., Gale, J.T.: Activation of the central nervous system induced by micro-magnetic stimulation. Nature Communications **4** (2013). DOI 10.1038/ncomms3463
35. Pashut, T., Wolfus, S., Friedman, A., Lavidor, M., Bar-Gad, I., Yeshurun, Y., Korngreen, A.: Mechanisms of magnetic stimulation of central nervous system neurons. PLOS Computational Biology **7** (2011). DOI 10.1371/journal.pcbi.1002022
36. Pikov, V., Arakaki, X., Harrington, M., Fraser, S.E., Siegel, P.H.: Modulation of neuronal activity and plasma membrane properties with low-power millimeter waves in organotypic cortical slices. Journal of Neural Engineering **7**(4) (2010). DOI 10.1088/1741-2560/7/4/045003
37. Rose R. M.; Hindmarsh, J.L.: The assembly of ionic currents in a thalamic neuron. I. The three-dimensional model. Proceedings of the Royal Society B: Biological Sciences **237** (1989). DOI 10.1098/rspb.1989.0049
38. Saltelli, A., Ratto, M., Andres, T., Campolongo, F., Cariboni, J., Gatelli, D., Saisana, M., Tarantola, S.: Global sensitivity analysis. The primer. Wiley (2008). DOI 10.1002/9780470725184.ch6
39. Saunders, R.D., Jefferys, J.G.R.: A neurobiological basis for elf guidelines. Health Physics **92**(6) (2007). DOI 10.1097/01.HP.0000257856.83294.3e
40. Schmid, G., Goychuk, I., Hänggi, P.: Effect of channel block on the spiking activity of excitable membranes in a stochastic hodgkin-huxley model. Physical biology **1**(1-2) (2004). DOI 10.1088/1478-3967/1/2/002
41. Seely, J., Crotty, P.: Optimization of the leak conductance in the squid giant axon. Physical Review E **82** (2010). DOI 10.1103/PhysRevE.82.021906
42. Shampine, L.F., Reichelt, M.W.: The matlab ode suite. SIAM Journal on Scientific Computing **18**(1) (1997). DOI 10.1137/S1064827594276424
43. Shannon, C.E.: A mathematical theory of communication. The Bell System Technical Journal **27**(3) (1948). DOI 10.1002/j.1538-7305.1948.tb01338.x
44. Shneider, M.N., Pekker, M.: Non-thermal mechanism of weak microwave fields influence on neurons. Journal of Applied Physics **114**(10), 104701 (2013). DOI 10.1063/1.4821027
45. Smith, G.D., Cox, C.L., Sherman, S.M., Rinzel, J.: Fourier analysis of sinusoidally driven thalamocortical relay neurons and a minimal integrate-and-fire-or-burst model. Journal of Neurophysiology **83**(1) (2000). DOI 10.1152/jn.2000.83.1.588
46. Sobol, I.M.: Sensitivity estimates for nonlinear mathematical models. Matematicheskoe Modelirovanie **2** (1990)
47. Strong, S., Koberle, R., Steveninck, R., Bialek, W.: Entropy and information in neural spike trains. Physical Review Letters **80** (1996). DOI 10.1103/PhysRevLett.80.197
48. Strukov, D.B., Snider, G.S., Stewart, D.R., Williams, R.S.: The missing memristor found. Nature **453** (2008). DOI 10.1038/nature06932
49. Virtanen, P., Gommers, R., Oliphant, T.E., Haberland, M., Reddy, T., Cournapeau, D., Burovski, E., Peterson, P., Weckesser, W., Bright, J., van der Walt, S.J., Brett, M., Wilson, J., Millman, K.J., Mayorov, N., Nelson, A.R.J., Jones, E., Kern, R., Larson, E., Carey, C.J., Polat, İ., Feng, Y., Moore, E.W., VanderPlas, J., Laxalde, D., Perktold, J., Cimrman, R., Henriksen, I., Quintero, E.A., Harris, C.R., Archibald, A.M., Ribeiro, A.H., Pedregosa, F., van Mulbregt, P., SciPy 1.0 Contributors: SciPy 1.0: Fundamental Algorithms for Scientific Computing in Python. Nature Methods **17** (2020). DOI 10.1038/s41592-019-0686-2
50. Wang, Y., Ma, J., Xu, Y., Wu, F., Zhou, P.: The Electrical Activity of Neurons Subject to Electromagnetic Induction and Gaussian White Noise. International Journal of Bifurcation and Chaos **27**(02) (2017). DOI 10.1142/S0218127417500304
51. Wilson, H.R.: Simplified Dynamics of Human and Mammalian Neocortical Neurons. Journal of Theoretical Biology **200**(4) (1999). DOI 10.1006/jtbi.1999.1002
52. Wu, F., Ma, J., Zhang, G.: A new neuron model under electromagnetic field. Applied Mathematics and Computation **347** (2019). DOI 10.1016/j.amc.2018.10.087
53. Wu, F., Wang, C., Jin, W., Ma, J.: Dynamical responses in a new neuron model subjected to electromagnetic induction and phase noise. Physica A: Statistical Mechanics and its Applications **469** (2017). DOI 10.1016/j.physa.2016.11.056
54. Xiu, D.: Fast Numerical Methods for Stochastic Computations: A Review. Communications In Computational Physics **5**(2-4) (2009). URL `http://global-sci.org/intro/article_detail/cicp/7732.html`
55. Xiu, D.: Stochastic Collocation Methods: A Survey. Springer International Publishing (2016). DOI 10.1007/978-3-319-11259-6_26-1
56. Xu, Y., Jia, Y., Wang, H., Liu, Y., Wang, P., Zhao, Y.: Spiking activities in chain neural network driven by channel noise with field coupling. Nonlinear Dynamics **95** (2019). DOI 10.1007/s11071-018-04752-2
57. Xu, Y., Ying, H., Jia, Y., Ma, J., Hayat, T.: Autaptic regulation of electrical activities in neuron under electromagnetic induction. Scientific Reports **7** (2017). DOI 10.1038/srep43452
58. Yang, Y., Ma, J., Xu, Y., Jia, Y.: Energy dependence on discharge mode of Izhikevich neuron driven by external stimulus under electromagnetic induction. Cognitive Neurodynamics (2020). DOI 10.1007/s11571-020-09596-4
59. Zhao, Y., Boulant, J.A.: Temperature effects on neuronal membrane potentials and inward currents in rat hypothalamic tissue slices. The Journal of Physiology **564**(1) (2005). DOI 10.1113/jphysiol.2004.075473

Figures

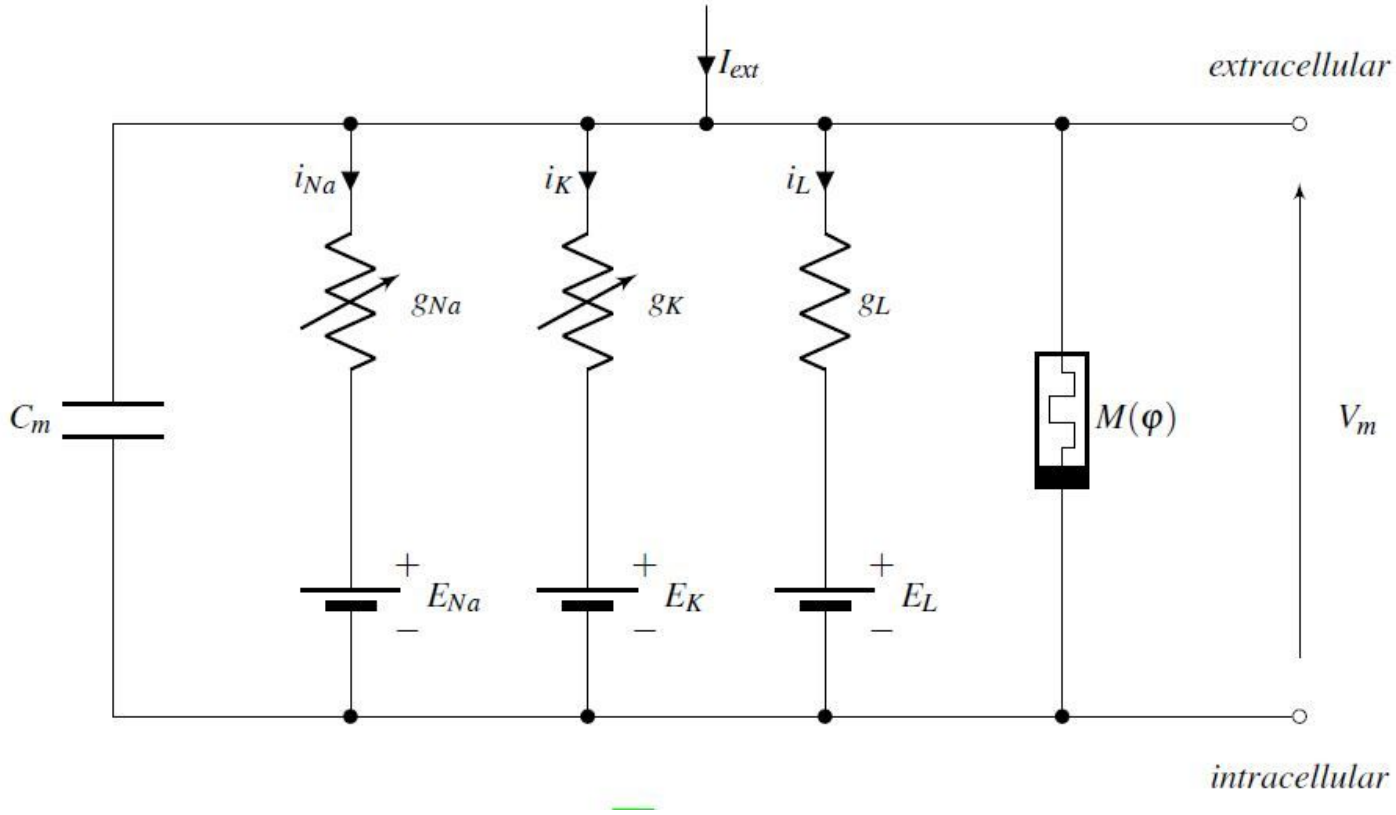

Figure 1

Hodgkin-Huxley neuron model equivalent electrical circuit [16] with the magnetic flux-controlled memristor, used to bridge the gap between the magnetic flux and the membrane potential and to enable the trans-membrane feedback current flow.

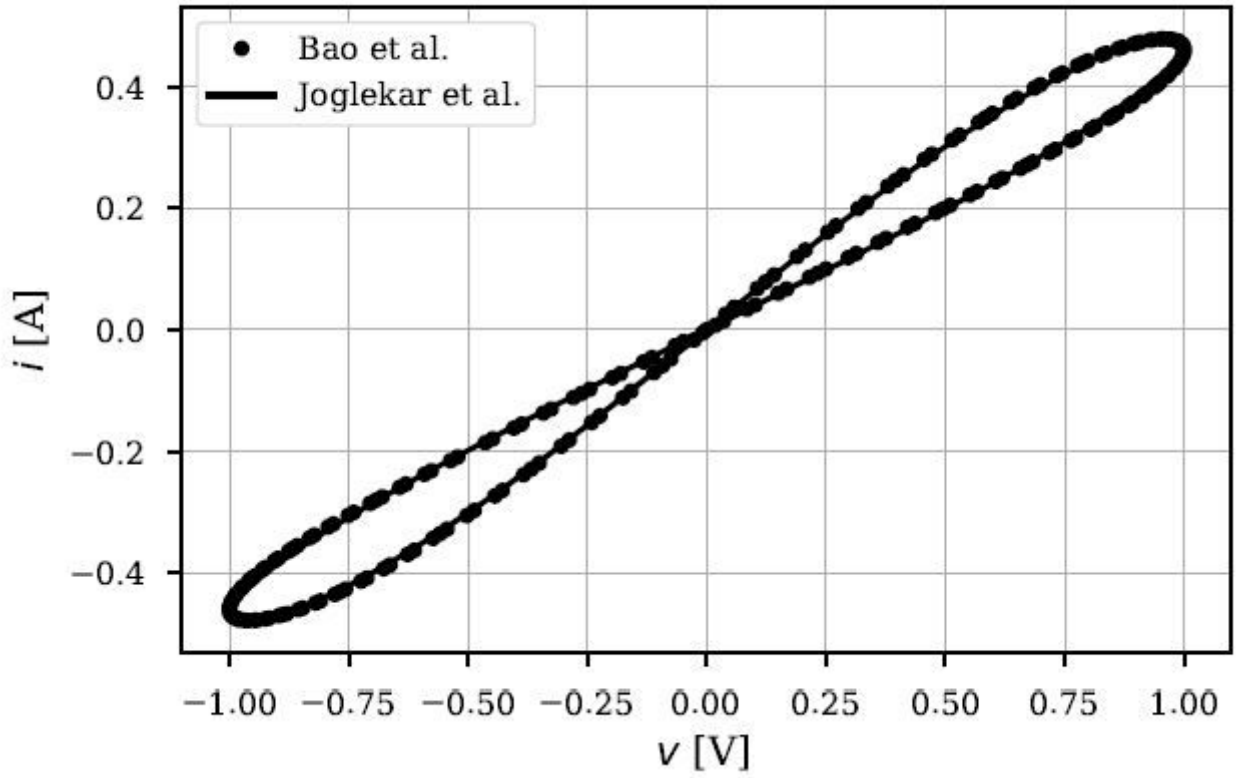

Figure 2

Visual representation of the iv characteristic compatibility between the non-linear polynomial approximatin of the memristor given in Bao et al. [1] and the actual memristor device realization [22] given in Joglekar et al.

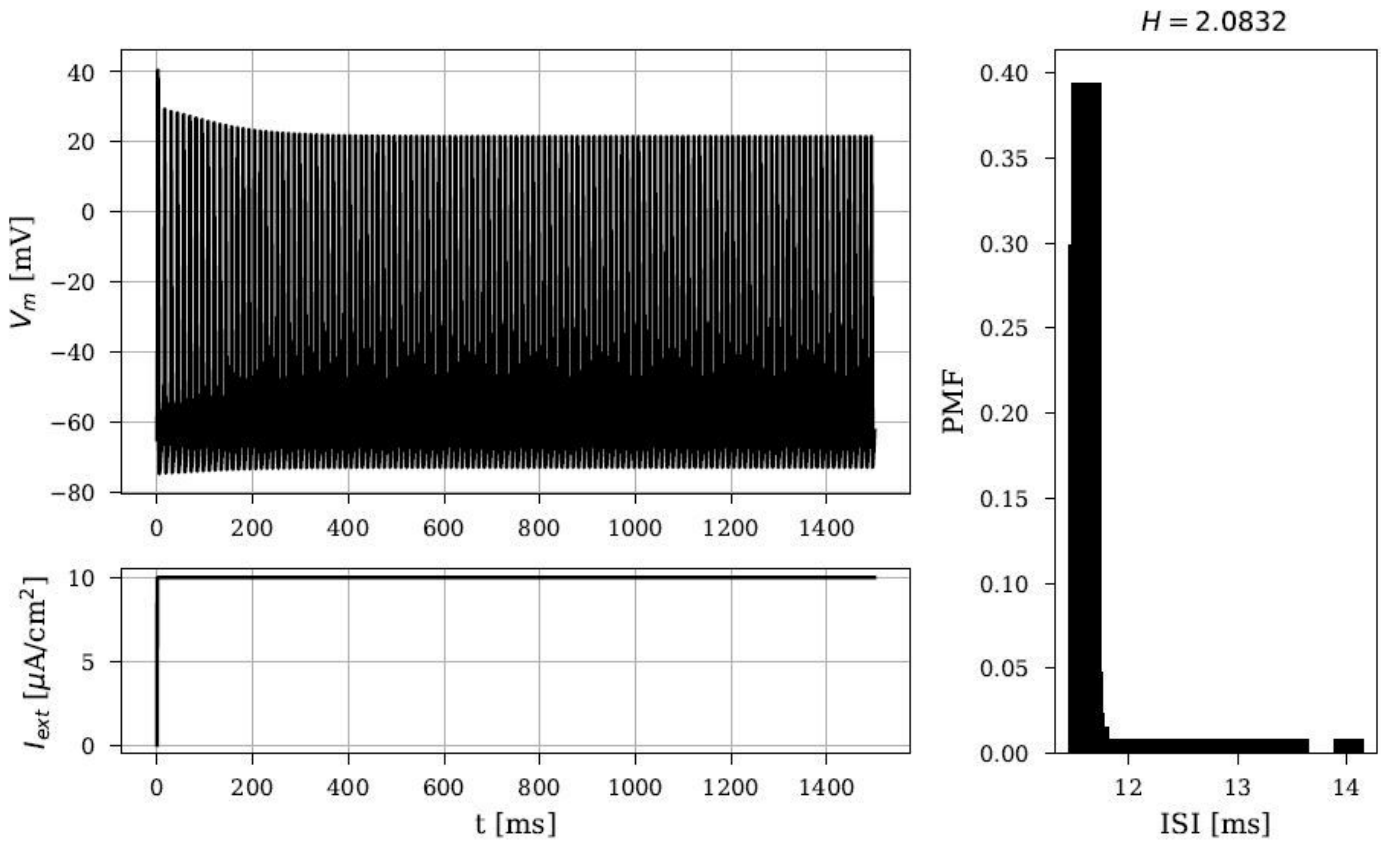

Figure 3

Action potential dynamics, Vm(t), shown in the top left subfigure, for the case of the direct current external stimulus, Iext (t), shown in the bottom left subfigure. Subfigure on the right depicts the probability density histogram (probability mass function) of ISIs, visually resembling an exponential distribution. Entropy amounts to H = 2:0832 for the number of bins determined via the Freedman-Diaconis rule [12].

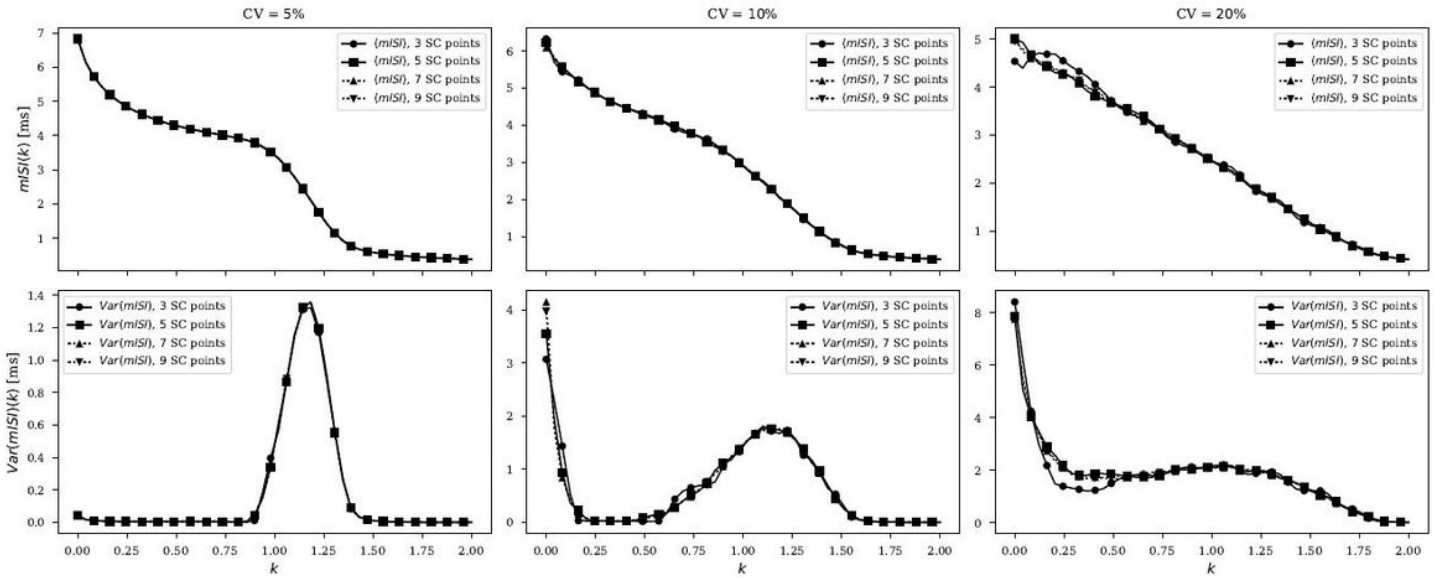

Figure 4

Convergence graph for the stochastic collocation method applied on bifurcation analysis of Hodgkin-Huxley neuron model for k 2 [0;2]. The convergence of the mean value for ISI is depicted in the first row, while the convergence for the variance is depicted in the second row for 4 levels of accuracy: 3, 5, 7 and 9 collocation points respectively. Each column depicts simulations for a different coefficient of variation, CV = 5, 10 and 20 per cent.

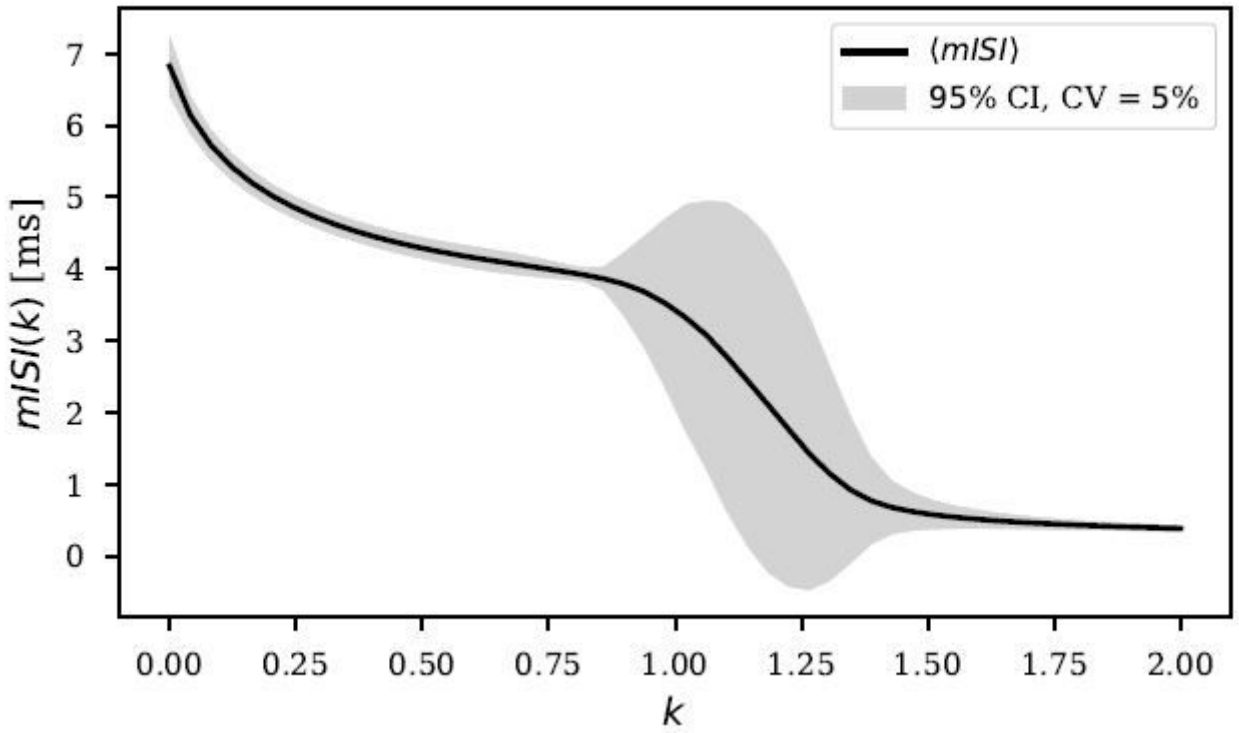

Figure 5

Mean ISI as a function of k inside 95 per cent confidence interval obtained via 5 collocation points and a coefficient of variation CV = 0:05.

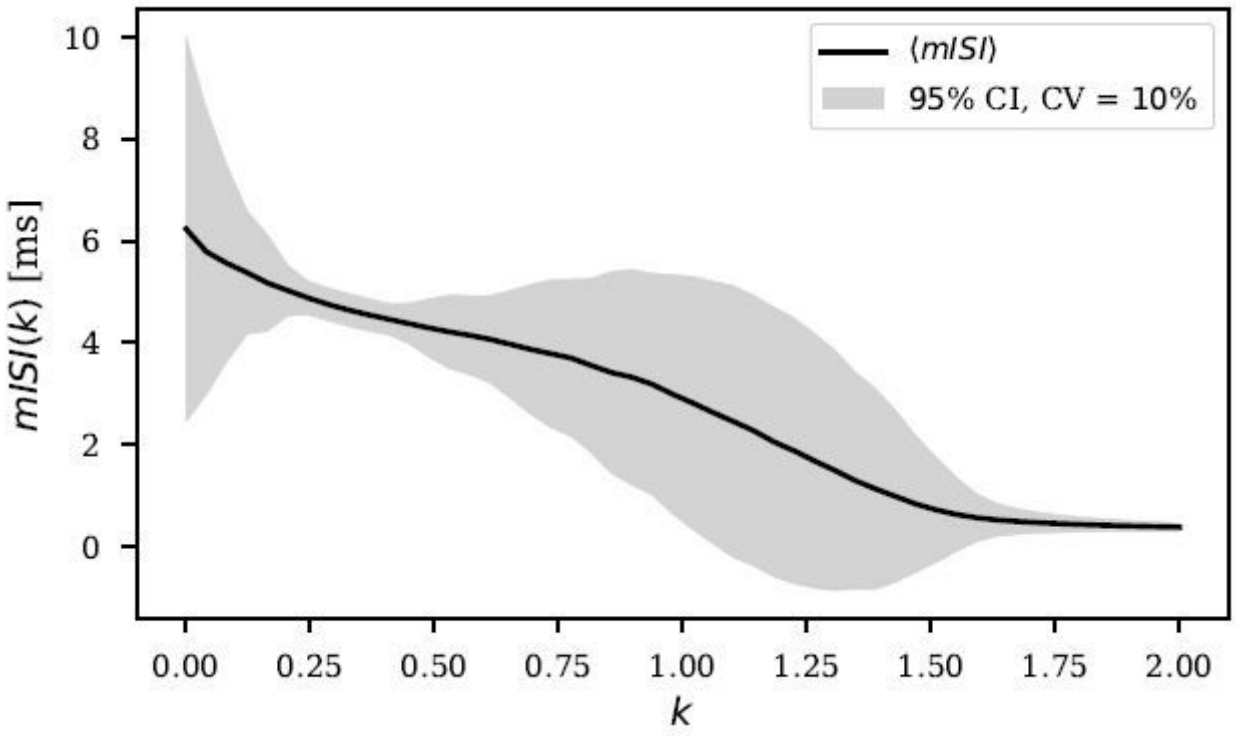

Figure 6

Mean ISI as a function of k inside 95 per cent confidence interval obtained via 5 collocation points and a coefficient of variation CV =0:1.

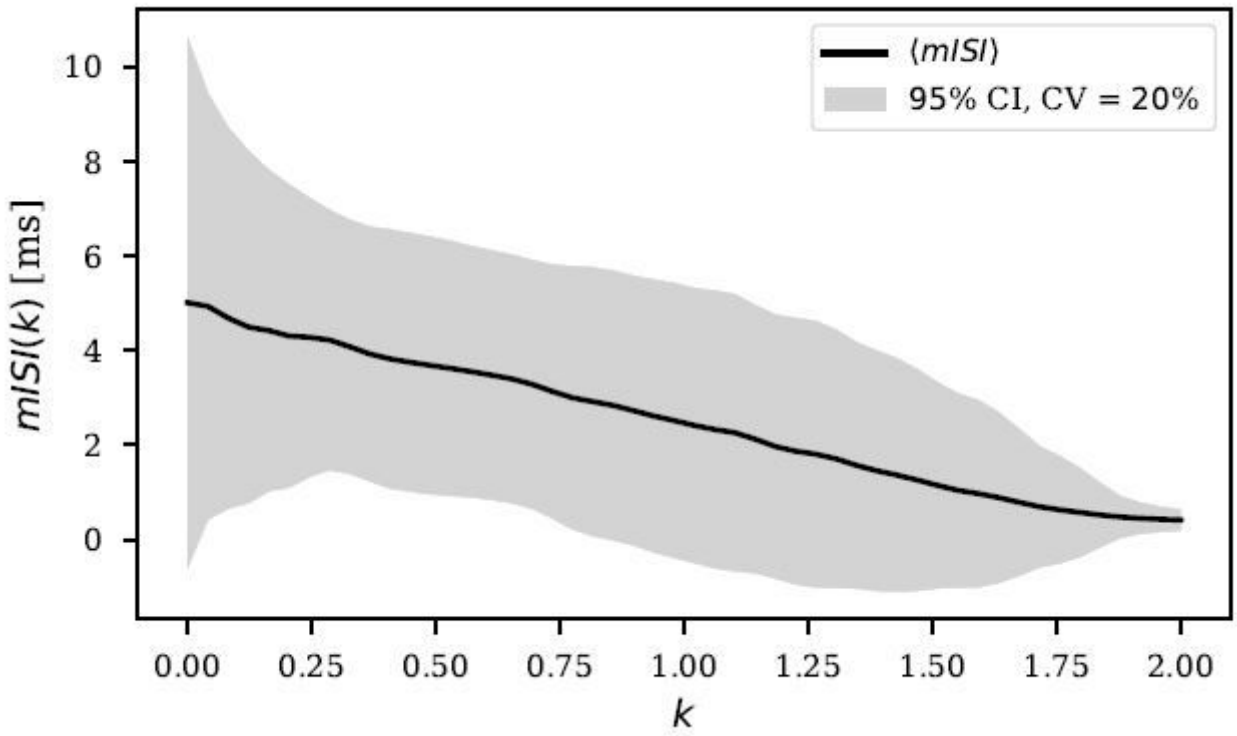

Figure 7

Mean ISI as a function of k inside 95 per cent confidence interval obtained via 5 collocation points and a coefficient of variation CV =0:2.

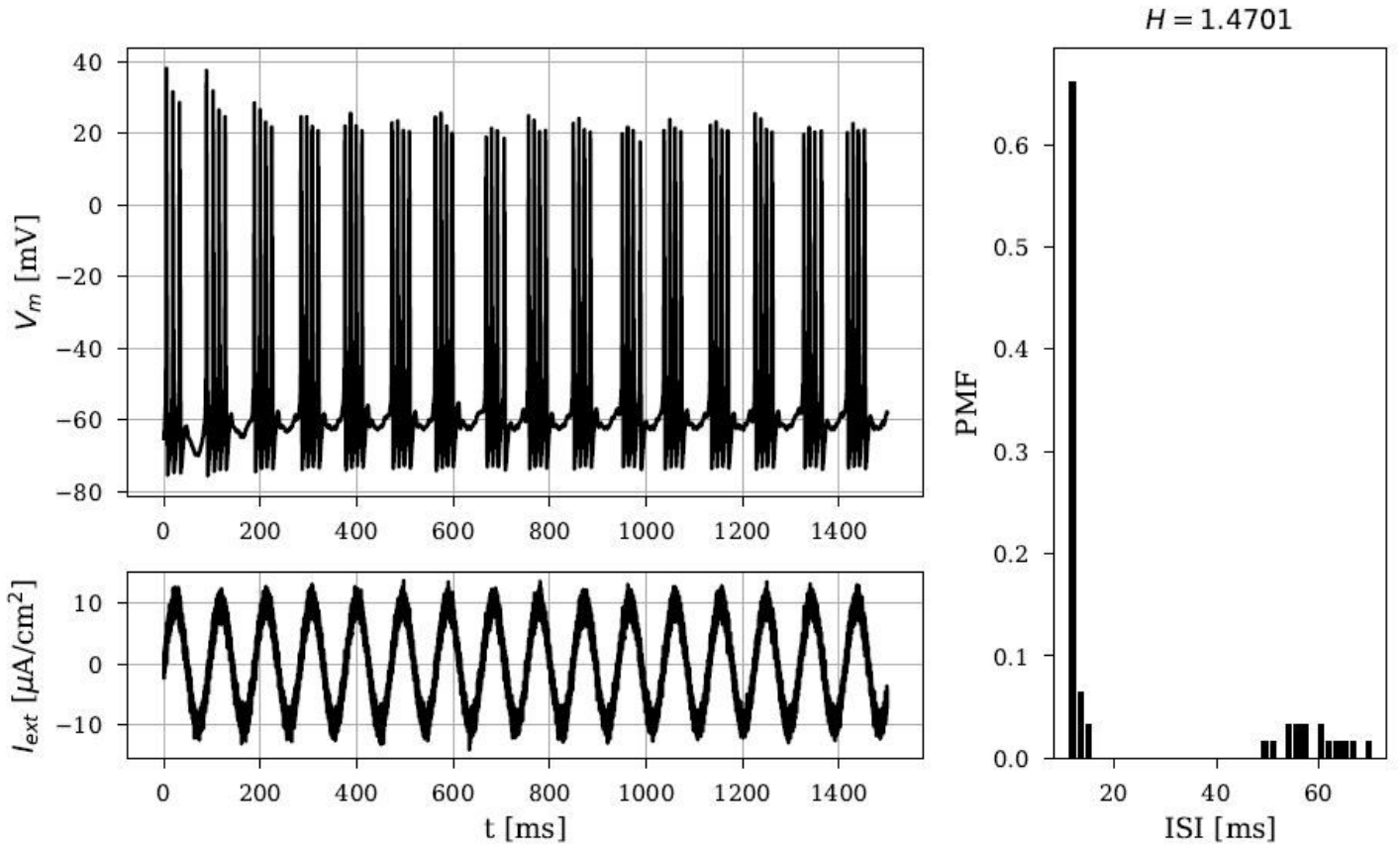

Figure 8

Action potential dynamics, Vm(t), shown in the top left subfigure, for the case of the direct current external stimulus, Iext (t), shown in the bottom left subfigure. Subfigure on the right depicts the probability density histogram (probability mass function) of ISIs. Entropy amounts to H = 1:4701 for the number of bins determined via the Freedman-Diaconis rule [12].

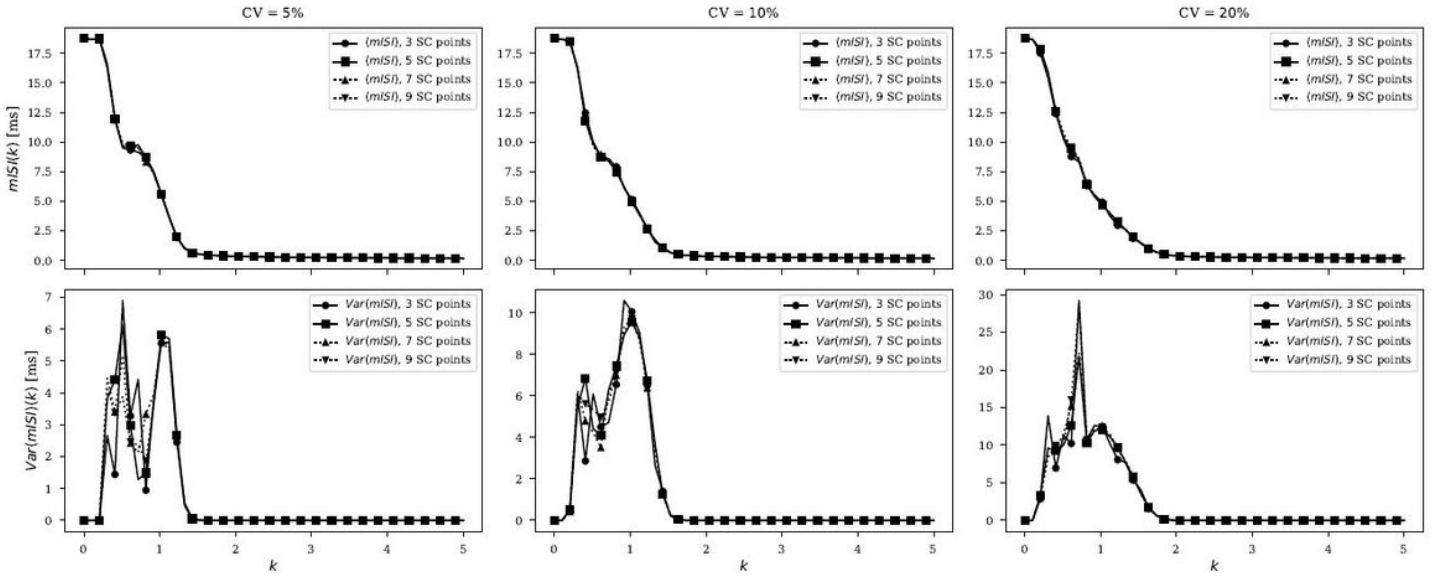

Figure 9

Convergence graph for the stochastic collocation method applied on bifurcation analysis of Hodgkin-Huxley neuron model for k 2 [0;5]. The convergence of the mean value for ISI is depicted in the first row, while the convergence for the variance is depicted in the second row for 4 levels of accuracy: 3, 5, 7 and 9 collocation points respectively. Each column depicts simulations for a different coefficient of variation, CV = 5, 10 and 20 per cent.

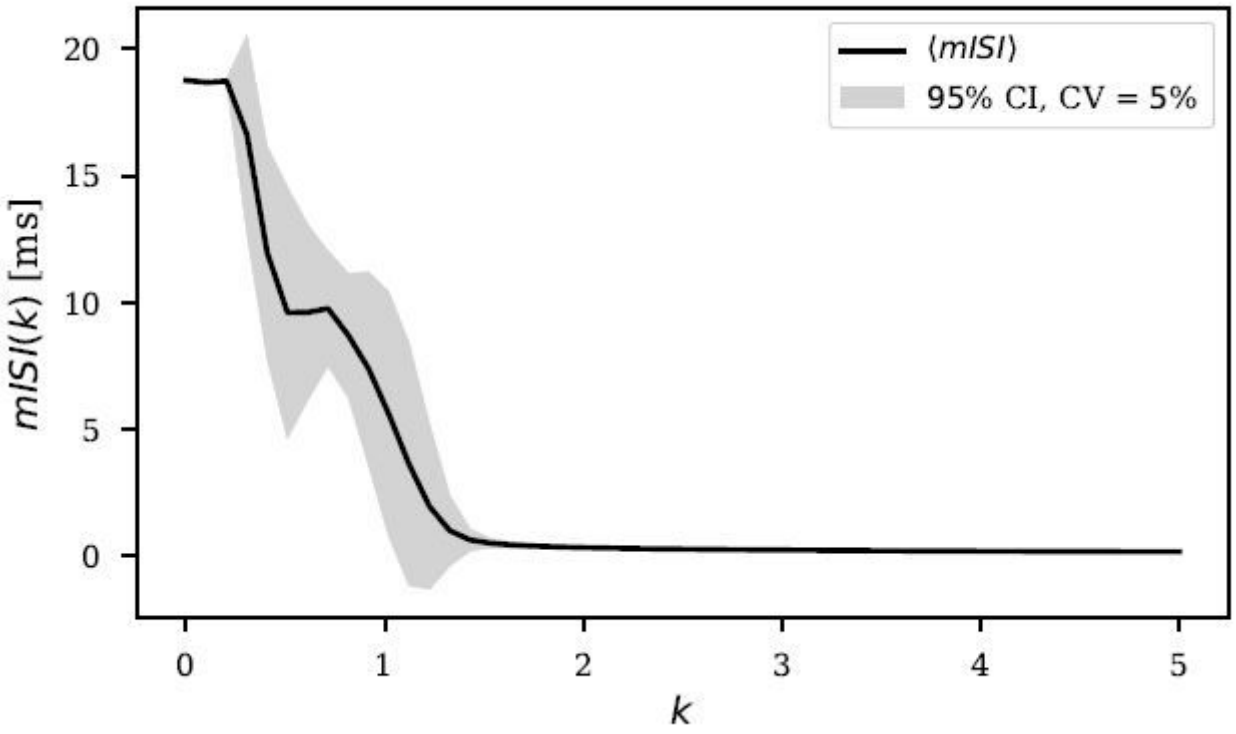

Figure 10

Mean ISI as a function of k inside 95 per cent confidence interval obtained via 5 collocation points and a coefficient of variation CV = 0:05.

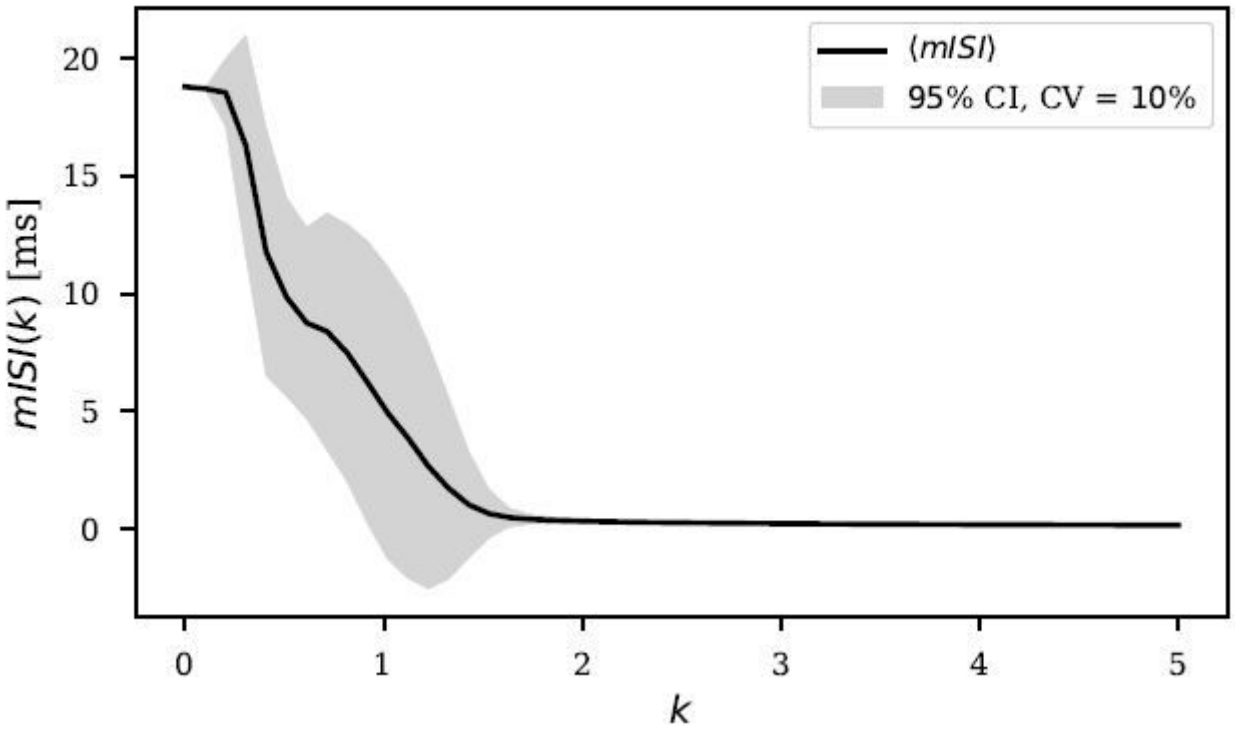

Figure 11

Mean ISI as a function of k inside 95 per cent confidence interval obtained via 5 collocation points and a coefficient of variation CV = 0:1.

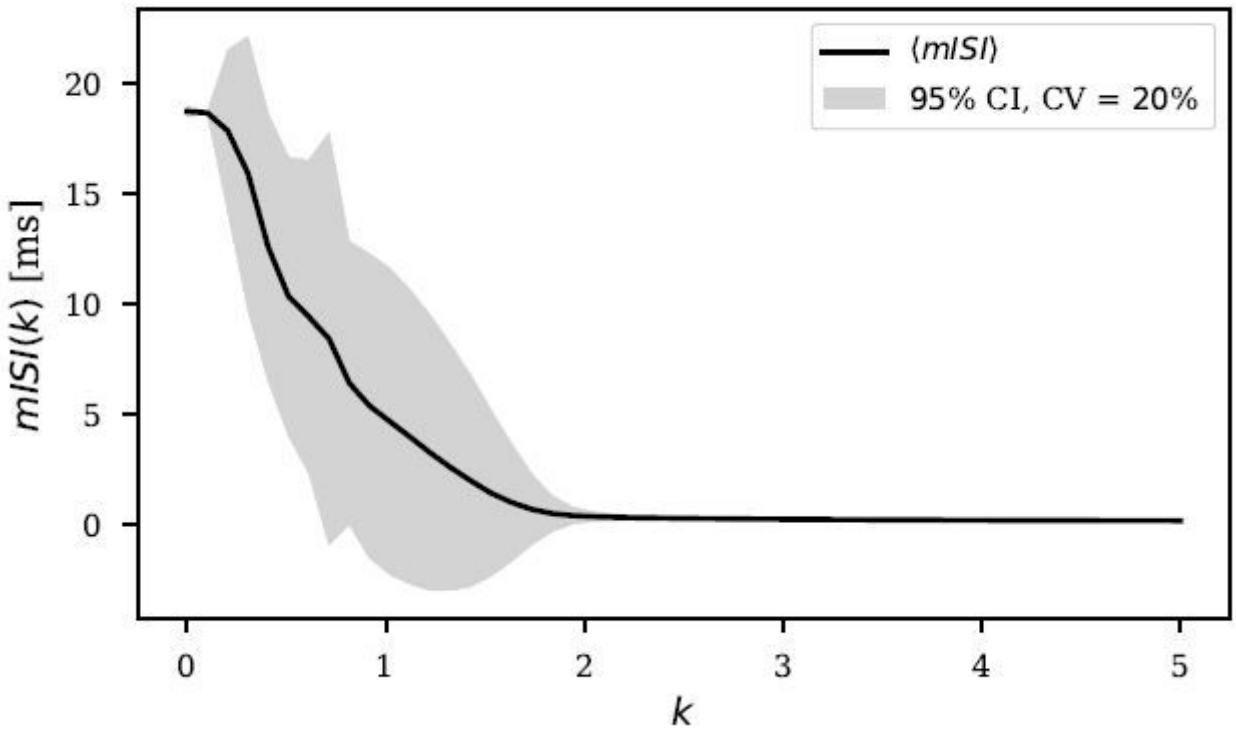

Figure 12

Mean ISI as a function of k inside 95 per cent confidence interval obtained via 5 collocation points and a coefficient of variation CV = 0:2.

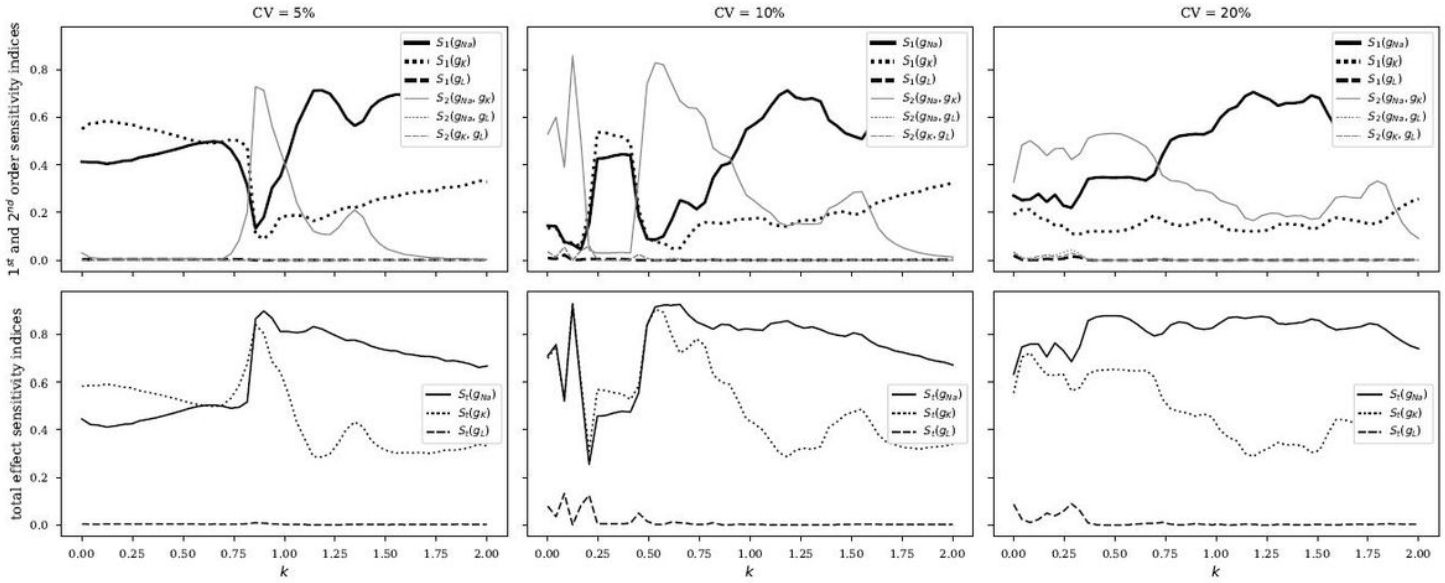

Figure 13

Variance-based sensitivity analysis for Hodgkin-Huxley neuron model under the influence of the electromagnetic induction. External neuronal stimulus for the case visualized in this figure is constant dc current. Upper row holds the first and the second order sensitivity indices of the output given ¯ gNa, ¯ gK and ¯ gL respectively, for the case of 5 collocation points. Lower row holds the total effect sensitivity indices of the output. Each column shows simulations for a different coefficient of variation.

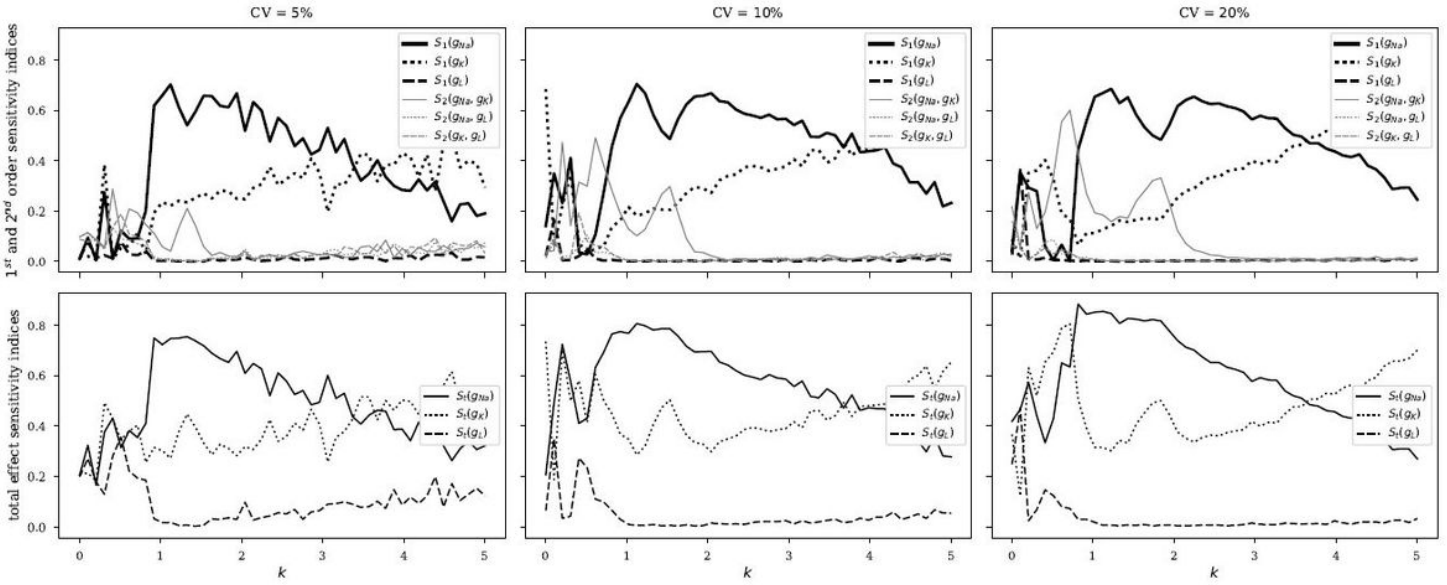

Figure 14

Variance-based sensitivity analysis for Hodgkin-Huxley neuron model under the influence of electromagnetic induction. External neuronal stimulus for the case visualized in this figure is noisy periodic current. Upper row holds the first and the second order sensitivity indices of the output given ¯ gNa, ¯ gK and ¯ gL respectively, for the case of 5 collocation points. Lower row holds the total effect sensitivity indices of the output. Each column shows simulations for a different coefficient of variation.